Decay and Mineralization of Mantis Shrimps (Stomatopoda: Crustacea)—A Key to Their Fossil Record

CEES H.J. HOF

Institute for Systematics and Population Biology, University of Amsterdam, P.O. Box 94766, 1090 GT Amsterdam, the Netherlands

DEREK E.G. BRIGGS

Department of Geology, University of Bristol, Wills Memorial Building, Queen's Road, Bristol BS8 1RJ, United Kingdom

PALAIOS, 1997, V. 12, p. 420–438

Experiments were carried out on decay and early diagenetic mineralization in the stomatopod Neogonodactylus *as a basis for the interpretation of fossil specimens of mantis shrimps.* Neogonodactylus *has a robust cuticle that is heavily mineralized in places in contrast to the decapods* Crangon *and* Palaemon, *which have been the subject of similar taphonomic experiments. Decay over 25 weeks resulted in a continuum of morphological stages: (1) swollen, due to osmotic uptake; (2) ruptured, as the exoskeleton split; and (3) partially decomposed, including weakening of the cuticle, decay of the soft-tissues, and disarticulation and fragmentation of the exoskeleton. Two categories of mineralization occurred; the precipitation of crystal bundles of calcium carbonate, and the replacement of soft-tissue and cuticle in calcium phosphate. Calcium carbonate formed as: (1) crystal bundles of various shapes; (2) crusts on the outside of the cuticle; and (3) an amorphous crystalline mass within the cuticle. The amount of soft-tissue mineralized in calcium phosphate increased throughout the experiment. In the later stages the hepatopancreas was often completely mineralized. Muscle tissue was replaced to a lesser extent and mostly in small fragments. Nerve ganglia were occasionally mineralized. The degree of mineralization was much greater than in decapod shrimps, presumably reflecting the higher calcium content and relatively phosphorus-rich cuticle of the stomatopod. The stages of morphological decay observed in these experiments can be identified in fossil stomatopods. SEM observations of fossil material have revealed phosphatized soft tissues similar to those found in the decaying carcasses. The experiments indicate that stomatopods have a relatively high fossilization potential. Their scarce and fragmentary fossil record must be a function of factors other than decay and degradation.*

INTRODUCTION

Taphonomic studies are crucial to reveal the factors that bias the fossil record of crustaceans. Although most interpretations of the taphonomy of crustaceans are based *a posteriori* on fossil occurrences (e.g., Glaessner, 1929; Mertin, 1941; Mundlos, 1975; Bishop, 1981), the amount of information obtained from experimental studies is increasing rapidly.

Both broad subdisciplines of taphonomy, i.e., biostratinomy and fossil diagenesis (see Müller, 1979), have been the focus of descriptive and experimental studies on decapod crustaceans. The empirical work of Schäfer (1951, 1972) included investigations of the decay and disintegration of brachyuran crabs in shallow sub- and intertidal environments of the North Sea. His work was invaluable in identifying some of the key variables in crustacean taphonomy (Brett and Baird, 1986; Plotnick, 1986). Allison (1986) demonstrated that freshly killed shrimps are very resistant to damage during transport, whereas they disarticulate rapidly following the onset of decomposition. Experimentally controlled laboratory and field experiments (Plotnick, 1986) on a modern caridean shrimp identified scavengers as the probable primary cause of carcass destruction. Further breakdown was caused by bacterial decomposition and disturbance by burrowing infauna. In a study on the fossilization potential of the mud crab *Panopeus,* Plotnick et al. (1988) showed that taphonomic processes are not invariant "filters" through which paleontological information is allowed to pass selectively (Behrensmeyer and Kidwell, 1985), but dynamic phenomena that change over ontogenetic, ecological and evolutionary time scales.

In decay experiments with a polychaete worm and the decapods *Nephrops* and *Palaemon,* Allison (1988) demonstrated that rapid burial and anoxia, traditionally considered to be the main prerequisites for exceptional preservation, may reduce the rate of decay but certainly do not stop it. Briggs and Kear (1993b, 1994) confirmed that early diagenetic mineralization was a critical factor in preserving soft-tissues. Under controlled experimental conditions, they observed the precipitation of crystal bundles of calcium carbonate, and the replacement of soft-tissue in calcium phosphate in the decaying shrimps *Crangon* and *Palaemon.* The nature of the experimentally mineralized soft tissues closely resembled those reported from fossils, indicating that similar processes were involved (Briggs et al., 1993). Baas et al. (1995) demonstrated that chitin is selectively preserved under the same experimental conditions.

Here we describe experiments on the stomatopod *Neogonodactylus oerstedii,* which complement previous work on decay and early diagenetic mineralization in decapod shrimps. This is only the second suite of experiments to document the extensive phosphatization of soft-tissues in the laboratory. The stomatopod cuticle is more robust than that in the decapods investigated, and it is heavily mineralized in places. Decay and mineralization under anaerobic conditions were monitored over a period of 25

0883-1351/97/0012-0420/$3.00

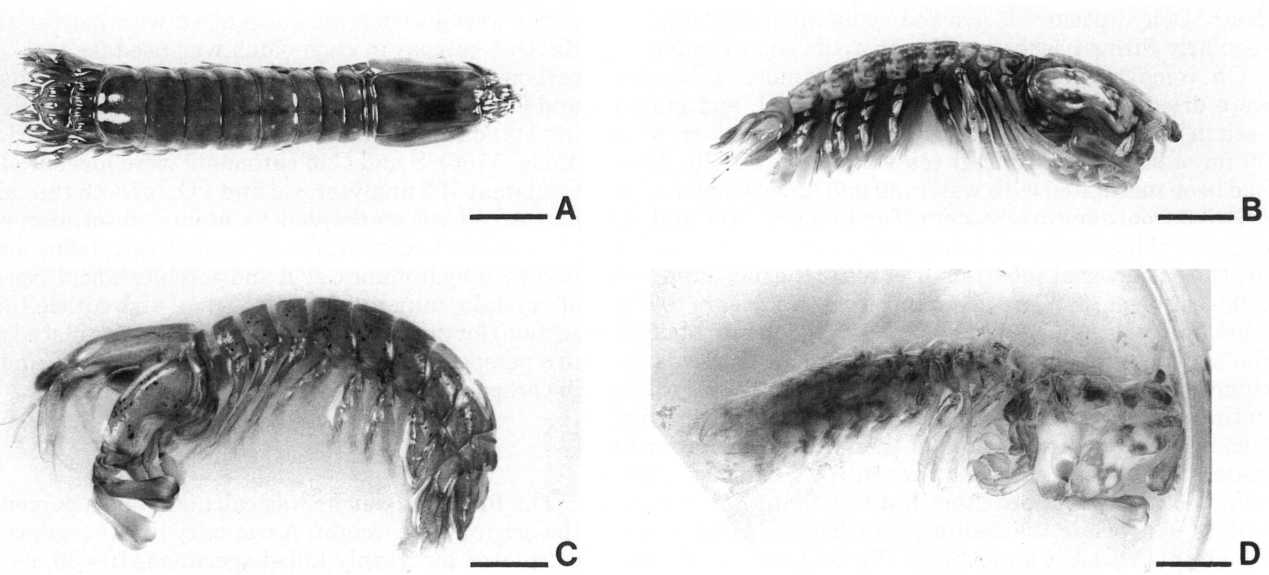

FIGURE 1—*Neogonodactylus oerstedii.* (A) Living, dorsal view. Scale bar is 7 mm. (B) Freshly killed, lateral view. Smashing limbs folded beneath the carapace. Scale bar is 8 mm. (C) After 3 days decay. Propodus of smashing limb unfolded, arthrodial membranes swollen especially between the posterior thoracic segments. Scale bar is 6 mm. (D) After 4 weeks decay. Cephalothorax separated from the trunk, smashing limbs detached after slight disturbance. Scale bar is 7 mm.

weeks. The results have general implications for the preservation of soft-tissues and cuticles, particularly in crustaceans. The morphological stages of decay identified in these experiments are evident in fossil stomatopods.

MATERIAL AND METHODS

Previous experiments investigated the effect of varying conditions on the decay of shrimps (Briggs and Kear, 1994). Here the focus is on how the morphology of the stomatopod influences its preservation potential. Hence all the experiments were carried out under the same conditions. The striking morphological and structural complexity of stomatopods allows the decay and mineralization of contrasting organs and tissues to be monitored in detail in a relatively small crustacean. The limited but well documented stomatopod fossil record facilitates comparative study.

Material

Stomatopods, also known as mantis shrimps, can be found on most of the world's tropical and subtropical coral reefs, sand, mud, and rubble-strewn coasts. These 10-to-350-mm-long crustaceans are active, alert, and highly visual predators exhibiting intense agonistic behavior while defending their burrows and cavities. Although seldom seen because of their secretive habits, stomatopods are often so numerous as to constitute a major predatory force in sub- and intertidal marine communities (Caldwell and Dingle, 1975, 1976). The most striking morphologic characteristic of stomatopods is the second thoracopod, which is developed as a large raptorial claw. The experiments were carried out on the stomatopod *Neogonodactylus oerstedii* (Hansen, 1895) (Malacostraca, Stomatopoda, Gonodactylidae) (Fig. 1A). *N. oerstedii* is the most common littoral stomatopod in the tropical and subtropical regions of the Western Atlantic, inhabiting a variety of habitats. It ranges in size from 8 to 76 mm. Males are dark, the body bluish with scattered yellow pigment in no particular pattern; females are light, the body cream colored with many scattered black chromatophores giving a speckled appearance overall. Their second thoracopod is a powerful smashing limb with heavily sclerotized dactylus and propodus. The carapace is characteristically divided into three fields by the paired parallel gastric grooves. The trunk is smooth and subcylindrical with inflated carinae on the last abdominal tergite and telson (for more details see Manning, 1969).

Living animals (n = 30; size range 0.39 g to 1.91 g) were obtained from the Fort Pierce area of Florida through the agency of the University of Sussex Centre for Neuroscience, Brighton, UK. The animals were held in aquaria in the Department of Geology, University of Bristol, until required. The aquaria were filled with 35–37‰ artificial sea water, which was aerated and filtered and kept at 23°C. To avoid severe agonistic fighting, hiding places were offered to the animals by placing rocks and short pieces of tubing (length 7 cm, diameter 1.8 cm) in a layer of fine gravel. Morbid or dead animals were not used for the experiments, nor were recently molted individuals. The animals were not fed for two days prior to the experiments.

Method

The stomatopods were killed by anoxia in order to ensure that specimens were complete and undamaged. They were placed in an empty beaker in the air-lock of an anaerobic cabinet. The air was pumped out of the chamber, which was then twice flushed with oxygen-free nitrogen and twice with an anaerobic gas mixture (CO_2, N_2, and H_2). Due to their tolerance to low oxygen levels, the animals were left in the chamber for 4 to 5 hours to ensure

death. Dehydration was avoided by damping the animals regularly with a tissue wetted with artificial sea water.

On removal from the anaerobic chamber, carcasses were dried by blotting with tissue, weighed, and placed each in a separate experimental vessel (ointment jar) with 50 ml of standard artificial sea water (ASW). The ASW had been inoculated with water (50 ml/l) and sediment (ca. 0.5 ml/l) from a natural system (Tay Estuary, Scotland) as a source of bacteria, and yeast extract (0.1 g/l) was added to act as a bacterial substrate. Details of the inoculum and composition of ASW are given in Briggs and Kear (1993a, 1994). pH was adjusted to 8.00 and oxygen saturation at the start was about 50%. The standard ASW recipe includes no phosphate, but analyzes showed that impurities in the salts used resulted in a phosphate concentration of 3.85 mg per liter. This is greater than the concentration in normal sea water (Lucas and Prévôt, 1991, listed values of 0.02 to 0.27 mg PO_4 per liter), but less than that in porewaters just below the sediment surface in Long Island Sound (FOAM site), for example (Ruttenberg and Berner, 1993, reported 10 mg per liter).

Thirty stomatopods were grouped into batches of five each, each batch destined to be sampled at a designated time. For each batch, six separate vessels—five with a carcass, the sixth identical, inoculated, but lacking a carcass—were sealed in a plasticized aluminium bag (method of Cragg et al., 1992) with Merck Anaerocult A (Merck Ltd., Poole, Dorset, UK.). This method creates anaerobic conditions within an hour (and corresponds to condition 1c of Briggs and Kear, 1993a, 1994). The vessels were incubated at 20° ± 0.5°C.

Sampling

The six batches were sampled after 3 days, and 1, 2, 4, 8, and 25 weeks, respectively. The color of the ASW was noted, and the presence or absence of bacterial films at the air interface and on the bottom of the jar was recorded by visual inspection. The pH and oxygen content of the ASW were measured (procedures and instruments as in Briggs and Kear, 1993a). The morphologic sequence of the decay state was recorded using a binocular microscope. Special attention was paid to the morphological and structural condition of distinctive body parts like the raptorial limbs, the carapace, and the telson. The wet and dry weight of 4 of the 5 carcasses were measured as in Briggs and Kear (1994). One carcass of each batch was stored in the freezer for future analyses of organic composition (see Appendix).

All of the sampled carcasses were examined using a binocular microscope. Two carcasses in each batch were selected for examination with the scanning electron microscope (SEM), with mineralization as a prime target. Samples for SEM examination were coated in gold and examined at 7–10 kV. Mineralized parts and representative pieces of the cuticle from these two carcasses were analysed by electron microprobe (EM). Backscatter images of some of the EM samples were photographed to document the mineralization patterns in and on the cuticle.

Chemical Analysis

Specimens for chemical analysis (Appendix) were oven dried on glass-fiber filter paper and then specimen plus paper were powdered/homogenized with mortar and pestle. One carcass in each batch was used for total organic carbon (TOC), S, and CHN ratio analyses, and one for Ca and PO_4 analyses. TOC and CHN ratios were analyzed using standard methods (Elemental Analyzer "Carlo Erba" Model 1106). S and C in carbonate were measured with a Coulamat 702 analyzer. Ca and PO_4 (of both the carcasses and ASW) were analyzed by atomic absorption spectrophotometry and colorimetry, respectively, following digestion with hydrofluoric acid and perchloric acid. Specimens of crystals, mineralized soft-tissue, and cuticle (in cross-section) for analysis in the microprobe were placed in holes in a perspex plate, immersed in resin, polished, and coated in carbon.

Statistical Comparison

The final wet weight was calculated as a percentage of the original wet weight. A wet : dry linear regression was calculated for freshly killed specimens ($n=36$, $r^2=0.937$). This was used to predict initial "baseline" dry weights. Final dry weights were expressed as a percentage of these "baseline" values. Data were processed using the statistical options of Microsoft Excel 4.0 and the statistical package SYSTAT 5.21. A one-way analysis of variance (Fully Factorial, Bonferroni mean comparison) was performed to examine the weight changes between the different time intervals. A two-way analysis of variance (Fully Factorial), was used to compare the decay rate of the shrimp *Crangon* in the experiments of Briggs and Kear (1994), with that of the stomatopods. In this analysis only the data for corresponding time intervals were used. The data from the chemical analyses were not subjected to statistical analysis due to the small number of samples ($n=1$ for each sample batch). All chemical analyses were repeated on a second sample from the same specimen in order to minimize error. The data for weights and pH are presented in the Appendix, which also identifies the specimens that were used for particular analyses.

MORPHOLOGICAL STAGES OF DECAY

Disintegration of the mantis shrimp took place in a sequence of morphological stages. These stages, which are based on detailed examination of all five specimens in each sample batch, are broadly similar to those in decaying decapod shrimps (Briggs and Kear, 1994). Hence the emphasis in what follows is on the features that distinguish stomatopods.

Freshly killed.—Killing resulted in no significant changes in the appearance of the stomatopod (Fig. 1A, B). When observed in ASW, the color pattern remained the same, the body was stretched, the antennules were directed anteriorly as were the antennae, the scaphocerites remained slightly curved backwards towards the body, the raptorial limbs were folded underneath the carapace, the walking legs were stretched, the pleopods hung loosely underneath the abdomen, and in most carcasses, the uropods were spread laterally.

3 days.—The colors faded. The carapace lifted slightly anteriorly due to osmotic uptake. The arthrodial membranes of the body showed swelling, particularly those separating the last 4 thoracic tergites. Osmotic pressure

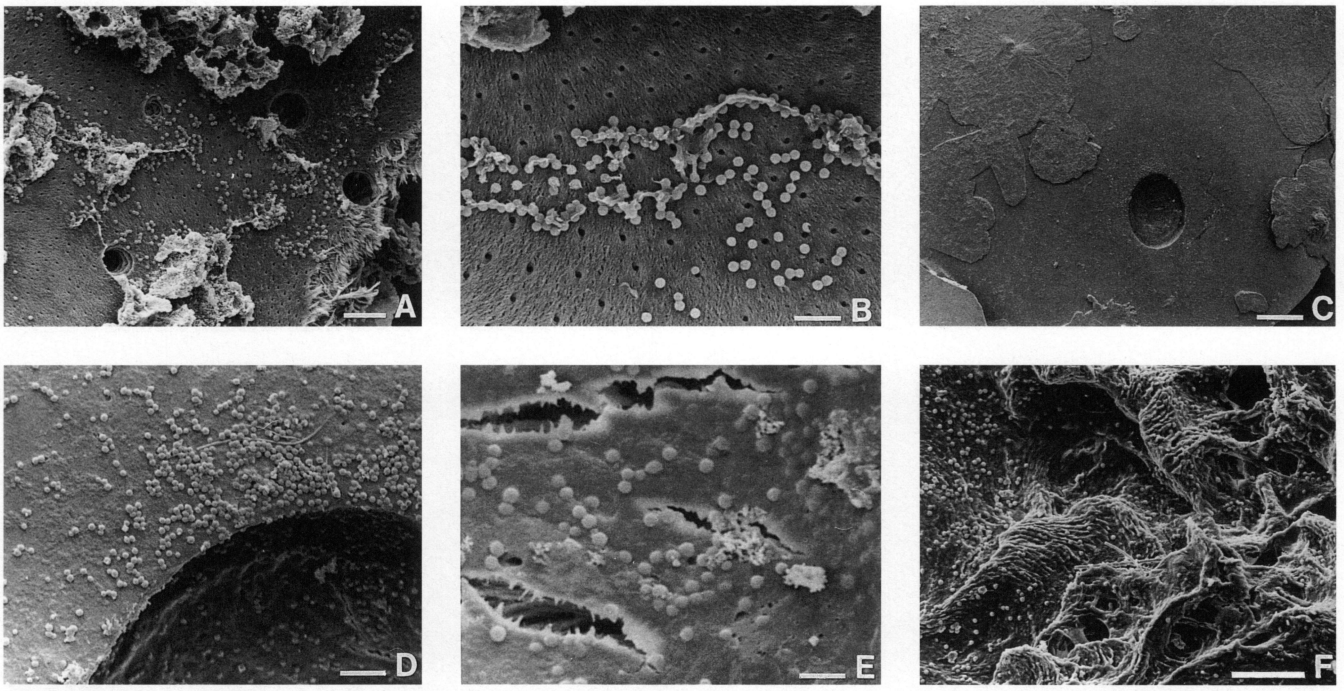

FIGURE 2—SEM illustrations of microbial activity after 8 weeks decay. (A) Bacteria decaying soft-tissue on the inner surface of the merus of a smashing limb. Scale bar is 10 μm. (B) Detail of (A) showing bacteria attached to soft-tissue fibers. Scale bar is 4 μm. (C) Bacterial degradation of the outer surface of the cuticle of an abdominal tergite, creating typical circular depression. The depression is surrounded by crystal crusts. Scale bar is 100 μm. (D) Detail of (C) showing concentrations of bacteria on cuticular surface around the depression. Scale bar is 10 μm. (E) Detail of (C) showing bacteria on the floor of the depression. Scale bar is 4 μm. (F) Fungal degradation, and bacteria, on the outer surface of one of the inflated carinae of the telson. Scale bar is 20 μm.

turned most of the appendages rigid. The raptorial limbs pointed obliquely downwards and unfolded, the propodus making an angle of about 90° with the merus (Fig. 1C). The intestines and body muscles were a slimy mass but still showed some coherence. One of the five carcasses became buoyant, the abdomen hanging down. All were still firm and remained intact when moved.

1 week.—The cuticle of the body turned transparent, females with a yellowish sheen, males with an orange sheen. The arthrodial membranes separating the last 4 thoracic tergites ruptured and those of the abdomen showed swelling, except that separating the last abdominal tergite and telson. The appendages were flexible, the walking limbs hanging down, the scaphocerites and pleopods loosely attached. The carapace became brittle. In some carcasses, the ventral side of the telson and the cuticle between the dorsal carinae became very soft and could be penetrated easily with a sharp object. Most of the carcasses lost their appendages when disturbed and the body divided, usually between the fifth and sixth thoracic tergites. The intestine and muscles were a fluid mass which lost its identity when the carcass was filtered.

2 weeks.—The arthrodial membrane between most of the tergites ruptured. The appendages remained loosely attached to the body. The cuticle was soft, except that of the propodus and dactylus of the raptorial limbs. The thinnest cuticle was destroyed by filtering; e.g., only the fringe of setae on the pleopods remained. Only the more sclerotized margins of the thoracic and abdominal tergites remained firm. On the external surface of the trunk cuticle, small circular indentations were evident (Fig. 2C). A striking pattern of cuticle degradation was observed on the inner surface of the telson (Fig. 3D, E, F). The helicoidal structure of the microfibrillar layers of the endocuticle was exposed, revealing the typical spiralling pattern of microfibrils. Other degradation phenomena were developed on the inner surface of an abdominal sternite (Fig. 3I). The slightest disturbance resulted in fragmentation of the body tergites and separation of the appendages. The appendages themselves, however, remained largely intact. The intestine and muscles were clearly visible through the transparent cuticle, but they disintegrated when disturbed.

4 weeks.—The carcasses sampled at 4 weeks showed remarkable variation in the state of morphological decay. Two, both with a relatively high initial weight (see Appendix 1), remained dark in color and retained a more robust cuticle than the others, although the internal features had almost disappeared. The remaining carcasses all appeared virtually intact but disintegrated with the slightest movement. The heavy raptorial limbs dropped off as did most of the other appendages. The body divided, initially between the last thoracic tergites (Fig. 1D). In some cases, the sixth abdominal somite remained attached to the telson. In one carcass the carapace separated from the body and disarticulated into the three distinct longitudinal fields. In two carcasses, the cornea of the eyes fractured, releasing the dark pigment. The muscle and intestines disintegrated when disturbed.

8 weeks.—Although very fragile, the carcasses remained complete and intact. The muscles were clearly visible through the transparent cuticle. The carcasses only disin-

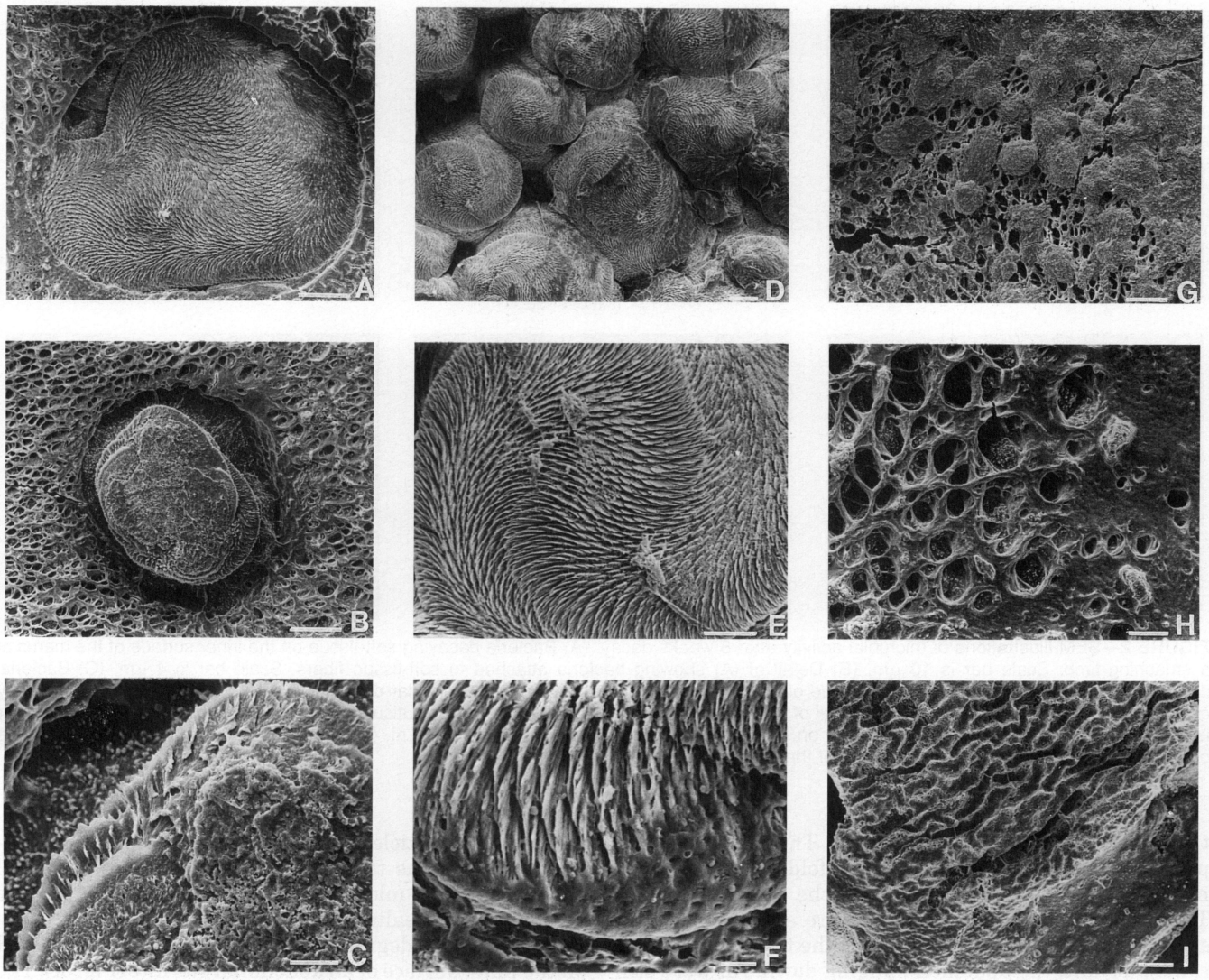

FIGURE 3—SEM illustrations of degradation affecting the endocuticle. (A) Circular pit on the lateral inner surface of an abdominal tergite (25 weeks). The spiral pattern reflects the helicoidal structure of the microfibrillar layers of the endocuticle. Scale bar is 40 μm. (B) A column of several endocuticular layers remains after annular degradation of the endocuticle on the same tergite. The surrounding area shows a sponge-like structure. Scale bar is 40 μm. (C) Detail of (B). Scale bar is 10 μm. (D) Cluster of endocuticular column-like remains inside a telson (2 weeks). Scale bar is 40 μm. (E) Detail of the surface of one of the columns from (D). Scale bar is 20 μm. (F) Detail of the margin of one of the columns from (D). Scale bar is 4 μm. (G) Sponge-like inner surface of the same tergite illustrated in A-C. Scale bar is 40 μm. (H) Spongy layer of the same tergite infilled in places with probably amorphous crystalline material. Scale bar is 20 μm. (I) Labyrinthine degradation on the inner surface of an abdominal sternite (2 weeks). Scale bar is 40 μm.

tegrated when they were disturbed. The morphological features that survive were determined by the nature of the mineralization (and are described in the section on mineral precipitation). The firmness of the carcass likewise depended on the extent of mineralization.

25 weeks.—The carcasses remained complete. Some of the limbs fell off due to their weight, usually the heavy raptorial limbs. Mineral formation gave some carcasses a degree of rigidity. The setae remained intact and the propodus and dactylus of the raptorial limbs were still robust. One carcass displayed remarkable decay patterns on the inner surface of the abdominal tergites (Fig. 3A, B, C), accompanied by reduction of the cuticle to a spongy network (Fig. 3B, G, H).

The descriptions of the morphological stages of decay are, of necessity, simplified. After one week the variation among carcasses in each sample batch increased. The state of the cuticle sometimes varied even within a single animal. However, the following simplified sequence could be recognized (see Fig. 5): (1) *Swollen*—within 3 days expansion of the internal tissues (due to osmotic uptake) led to the unfolding of the raptorial limbs and stretching of the arthrodial membranes; (2) *Ruptured*—by 1 week the exoskeleton started to split, either between the last three thoracic tergites or between the thorax and the abdomen; (3) *Partially decomposed*—by 4 weeks carcasses showed progressive weakening of the cuticle, decay of the soft-tissues, and disarticulation and fragmentation of the exoskeleton when disturbed. The connective tissue between the segments of the individual appendages, and between the telson and the last abdominal somite, was more decay-resistant than that elsewhere.

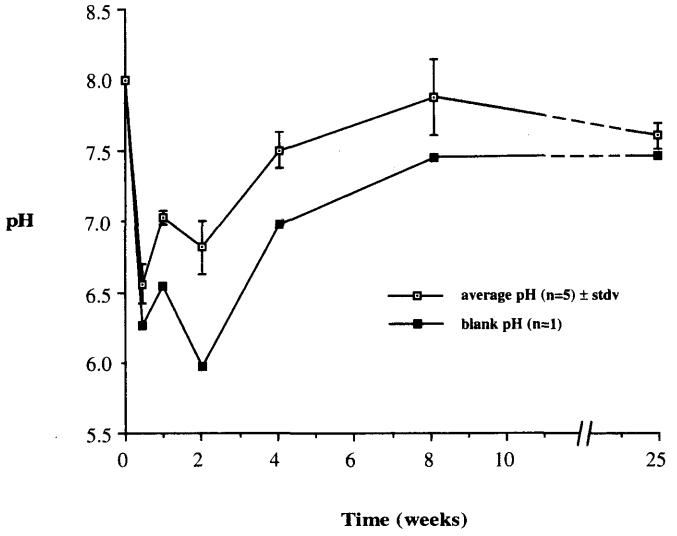

FIGURE 4—The variation in pH over time (see Appendix). The average pH recorded for vessels containing decaying carcasses (the vertical bars indicate the standard deviation) is compared with the values for the controls, which contained no carcass.

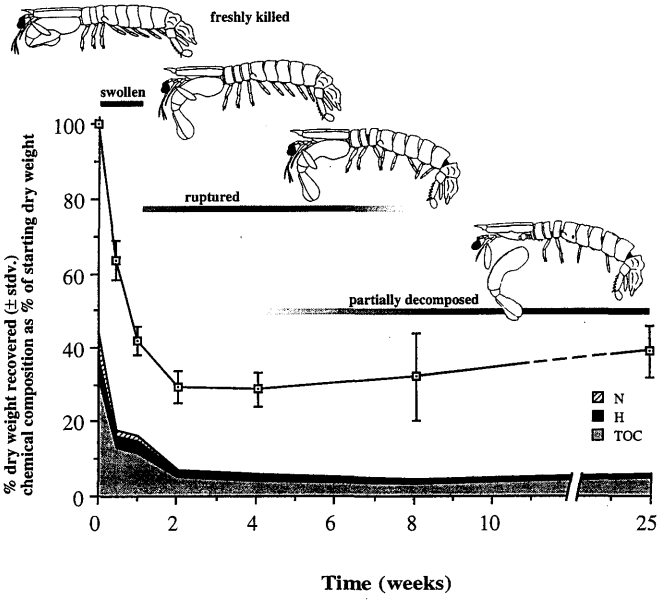

FIGURE 5 —Times through which stages of decay were observed in the decay experiments (the diffuse limits to the ranges indicate variation in the onset and persistence of stages from carcass to carcass). Percentage dry weight recovery (the vertical bars indicate the standard deviation, see Appendix), and variation in nitrogen, hydrogen, and organic carbon (expressed as a percentage of starting dry weight, see Table 1) over time.

MICROBIAL DEGRADATION OF THE CUTICLE

SEM observations revealed direct evidence of the impact of microbial activity on the cuticle. Bacteria were found on the inner surface (Fig. 2A), sometimes attached to fragments of muscle fiber (Fig. 2B). Circular pits began to appear on the cuticle within three days and were evident, varying in shape, diameter and depth (Fig. 2C) throughout the experiments. Concentrations of bacteria were often evident within and around these degradation phenomena (Fig. 2D, E). Microbial decay, particularly on the inner surface of the trunk tergites and telson, revealed the internal structure of the cuticle. Shallow subcircular depressions showed the helicoidally arranged microfibrils of the endocuticle (Fig. 3A). Sometimes a ring of cuticle was consumed by microbes, leaving a column of endocuticle (Fig. 3B). Bacteria were evident on the floor of the ring-shaped depression (Fig. 3C). Clusters of endocuticular columns (Fig. 3D) were sometimes formed by decay. These columns clearly revealed the helicoidal structure of the endocuticle (Fig. 3E), although bacteria were no longer evident on the surface (Fig. 3F). Very rarely the surrounding cuticle displayed a spongy (Fig. 3B, G, H) or labyrinthine (Fig. 3I) texture which also appeared to be bacterially induced. Bacterial decay has not been reported to reveal the helicoidal structure of the endocuticle before (A.C. Neville, pers. comm.).

Some specimens showed black spots or stains on the cuticle in life, which may have been fungal in origin. There is no evidence that these spots promoted decay, but they did form a suitable substrate for bacteria (Fig. 2F).

QUANTITATIVE CHANGES DURING DECAY

Oxygen Concentrations

Initial oxygen concentrations were ca. 50%. Throughout the experiments, the average oxygen level measured did not exceed 3% saturation. The combined effects of Merck Anaerocult® A and decay itself (Briggs and Kear, 1994) ensured that processes were O_2 limited and anaerobic almost from the outset.

pH

The pH of the ASW (Fig. 4, data in Appendix) fell from the initial value of 8.00 to a mean of 6.56 within 3 days. After 1 week, the pH had recovered to 7.03 but dropped again to 6.82 after 2 weeks. By 4 weeks the pH had risen to 7.51. It never returned to the starting value, reaching a maximum of 7.88 by 8 weeks and then falling to pH 7.61 after 25 weeks. The pH profile of the control (Fig. 4) shows a similar pattern, but with lower values. Thus the CO_2 introduced by the Anaerocult had a significant impact on pH levels. A fall in pH to below 6.5 has been recorded, however, around shrimps decaying anaerobically in aqueous experiments for 10 days where no Anaerocult was used.

Weight Changes

The rate of decay was quantified by monitoring the change in weight (Fig. 5, Appendix) and the chemical composition of the animal remains (Fig. 5, Table 1). No correlation was found between percentage weight loss (dry weight) and the initial weight of the carcass (correlation coefficient < 0.95).

Mean wet weight (see Appendix for data) increased to 115.1% of the starting weight within the first three days. This short period of osmotic uptake was followed by a steep decline to 60.7% after one week, and 34.6% after two. Thereafter, the mean wet weight remained similar, 32.6% after 4 weeks, 32.4% after 25 weeks. There was a small increase in week 8 up to 46.9%. Statistical analysis showed

TABLE 1—Composition of mantis shrimp *Neogonodactylus oerstedii* as weight % of starting dry weight (% start) and weight percent of remaining dry weight (% now). TOC is total organic carbon; $C\text{-}CO_3$ is carbon present as carbonate.

	TOC		$C\text{-}CO_3$		H		N		PO_4		Ca		S	
	% Start	% Now	% Start	% Now	% Start	% Now	% Start	% Now	% Start	% Now	% Start	% Now	% Start	% Now
Fresh	31.37		3.12		5.07		7.05		5.22		5.95		0.42	
3 days	12.96	22.47	—	—	3.05	3.04	1.64	2.84	5.61	7.99	4.06	5.78	0.44	1.07
Week 1	11.37	29.96	—	—	3.40	4.34	1.42	3.73	4.22	9.00	2.51	5.34	0.32	1.25
Week 2	5.05	14.89	0.56	1.66	1.36	2.07	0.49	1.46	4.88	15.12	2.03	6.30	0.14	1.05
Week 4	4.04	16.36	—	—	1.38	2.51	0.30	1.21	4.40	12.57	2.25	6.43	0.01	0.02
Week 8	3.14	21.74	0.20	1.40	1.10	3.29	0.21	1.47	5.37	13.42	2.94	7.35	0	0
Week 25	4.73	12.09	1.37	3.50	0.82	1.03	0.17	0.43	4.33	14.09	1.16	3.79	0	0

no significant change in wet weight after one week. The high standard deviations that characterize the wet-weight values (see Appendix) make it difficult to monitor decay in this way.

Dry weight (Fig. 5, see Appendix for data) is a much more reliable indication of the progress of decay (Briggs and Kear, 1994). Mean dry weight showed a rapid decline during the first two weeks. Just 63.5% of the initial dry weight remained after three days, 41.8% after 1 week, and 29.4% after 2 weeks. This rapid decline, which correlates with the rupturing of the carcass, was followed by a slight rise through 28.7% after 4 weeks, 32.1% after 8 weeks, to 38.9% after 25 weeks. This rise may be the result of mineral accumulation within the carcass.

CHEMICAL DEGRADATION

Changes in the composition of *Neogonodactylus* at successive sampling intervals can be expressed as a percentage of the starting dry weight (Fig. 5), or as a percentage of the material remaining (Table 1). 58.2% of the starting composition of *Neogonodactylus* consists of organic C, N, H, PO_4, C in carbonate, Ca, and S. The remainder is predominantly O with some minor elements. The starting CHN ratio of 1:1.92:0.19 changed through 1:1.61:0.11 (3 days), 1:1.72:0.11 (1 week), 1:1.66:0.08 (2 weeks), 1:1.83:0.06 (4 weeks), 1:1.8:0.06 (8 weeks), to 1:1.01:0.03 (25 weeks). TOC, H and N all showed a rapid initial decline, which correlates with rupturing of the carcass and major weight loss (Fig. 5). TOC dropped 20% to about 10% of the starting dry weight within a week. After this decline it more or less stabilized around 4% of the starting dry weight. H dropped from 5% to about 3% in the first week, after which it slowly decreased to 0.82% after 25 weeks. N showed a rapid decline from 7% to 1.64% within 3 days, reaching 0.17% after 25 weeks. C in CO_3 showed a much less pronounced decline. PO_4 remained a more or less constant percentage of the starting dry weight throughout the experiment. Ca declined steadily from an initial 5.95% to 1.16% of the starting dry weight after 25 weeks. The percentage of S reached zero after 8 weeks.

The composition of the carcasses expressed as weight percent of the remaining dry weight shows that organic C, PO_4 and Ca are the dominant components (Table 1). TOC remained at about 16 % from week 2. PO_4 showed an increase from 5.22% to an average of 14% from week 2 to 25. Ca remained at more or less the same percentage throughout.

MINERAL PRECIPITATION

Decay of the mantis shrimp carcasses was accompanied by the precipitation of minerals. The styles of mineralization fall into four broad but distinct categories: (1) crystal bundles of $CaCO_3$ that form within the carcass, particularly within the trunk segments and telson; (2) crystal crusts of $CaCO_3$ that form on the external surface of mainly the trunk segments; (3) microspheres of $CaPO_4$, which replicate the soft tissue, particularly the hepatopancreas and muscle fibers; and (4) finely crystalline $CaCO_3$, which precipitated within the cuticle of the trunk segments, and is only clearly visible when the cuticle is sectioned.

Crystal Bundles

Crystal bundles are aggregates of hundreds of micron-sized crystals (Buczynski and Chafetz, 1991). Those that precipitated in the mantis shrimp carcasses took a variety of forms including hemispheres (Figs. 6A-C, 8A-C), spheres (Fig. 8D), rods (Fig. 8D), dumbbells (Fig. 7A-C), and almond-shaped crystals (Fig. 7D-F). They are composed of calcium carbonate (Table 2) and formed in 40%, 60%, and 40% of the carcasses sampled at 4, 8, and 25 weeks respectively.

Hemispheres were initiated as layers of elongate crystals radiating from a marginal or central nucleus on the cuticle surface. As additional radiating crystals were added and the relief increased, a crystalline hemisphere formed (Fig. 6B). Those that formed on the carapace had a porous surface produced by the action of the microbes and tended to occur in clusters (Fig. 6B). Figure 6C shows the early stage of formation of two coalescing hemispheres. The hemispheres that occurred on the inner surface of the trunk cuticle formed mainly on the lateral area of the tergites (Fig. 8A), or on the margins of the sternites (Fig. 8B). Some of them showed a small depression or a series of irregular bumps in the center of the surface (Fig. 8C). The crystal hemispheres were all bright white in color. Complete spheres were rare and only found within the clusters of rods (Fig. 8D). They were made up of triangle-shaped crystals (Fig. 8F) and were whitish in color.

Rods were sometimes found projecting from the inner surface of the trunk tergites, but they occurred mostly in massive clusters inside the abdominal somites or the telson (Fig. 8D). In some cases, rods were found within and on the mineralized hepatopancreas (Fig. 10E). These rods were bundles of overlapping wedge-shaped crystals (Fig.

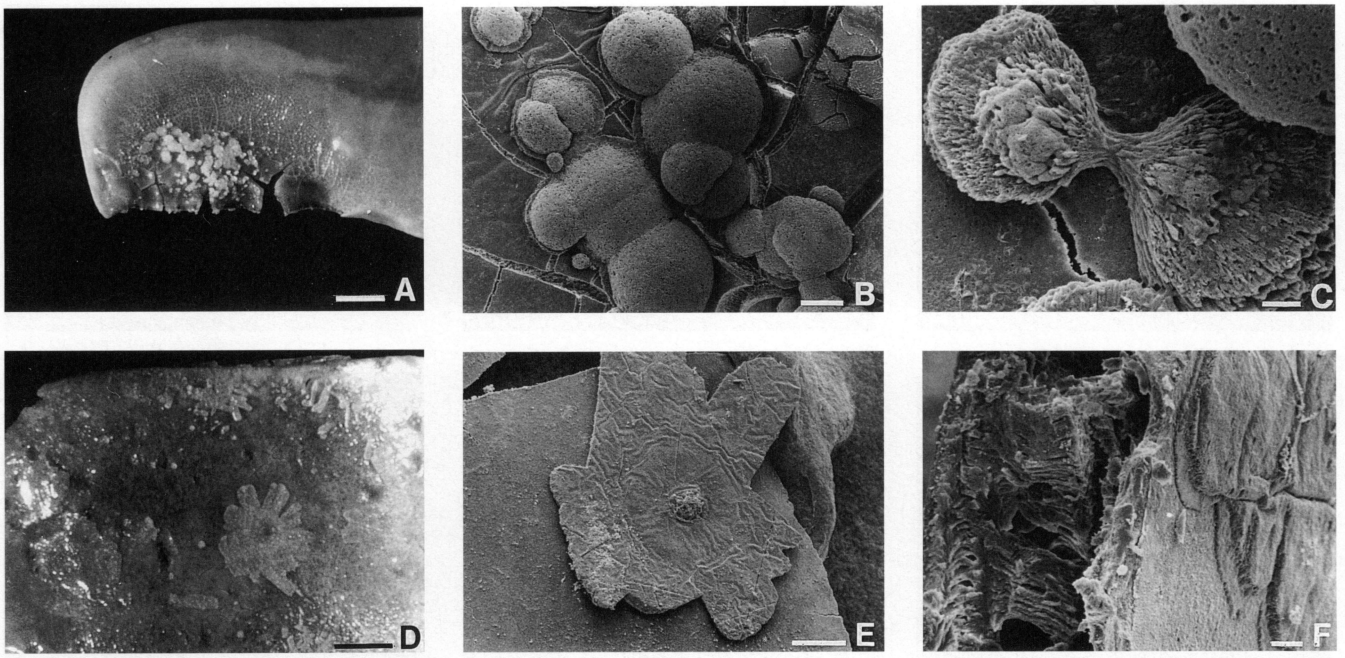

FIGURE 6—Styles of $CaCO_3$ mineralization. (A) Crystal bundles on the posterior ventral side of the right lateral field of a tergite (8 weeks). Scale bar is 0.5 mm. (B,C) SEM illustrations. (B) Crystal bundles shown in (A). Scale bar is 40 μm. (C) Detail of the radiating form of the crystal bundles. Scale bar is 4 μm. (D) Large rosette crystal bundle and smaller flat crystals on the outer surface of an abdominal tergite (25 weeks). Scale bar is 1 mm. (E,F) SEM illustrations. (E) Crystal bundle on outer surface abdominal tergite showing central nucleus (8 weeks). Scale bar is 40 μm. (F) Cuticle of abdominal tergite showing the cuticular layers (left) and a crystal crust on the surface (right) (8 weeks). The crust consists of two layers, a thin basal one and a slightly thicker upper one. Scale bar is 10 μm.

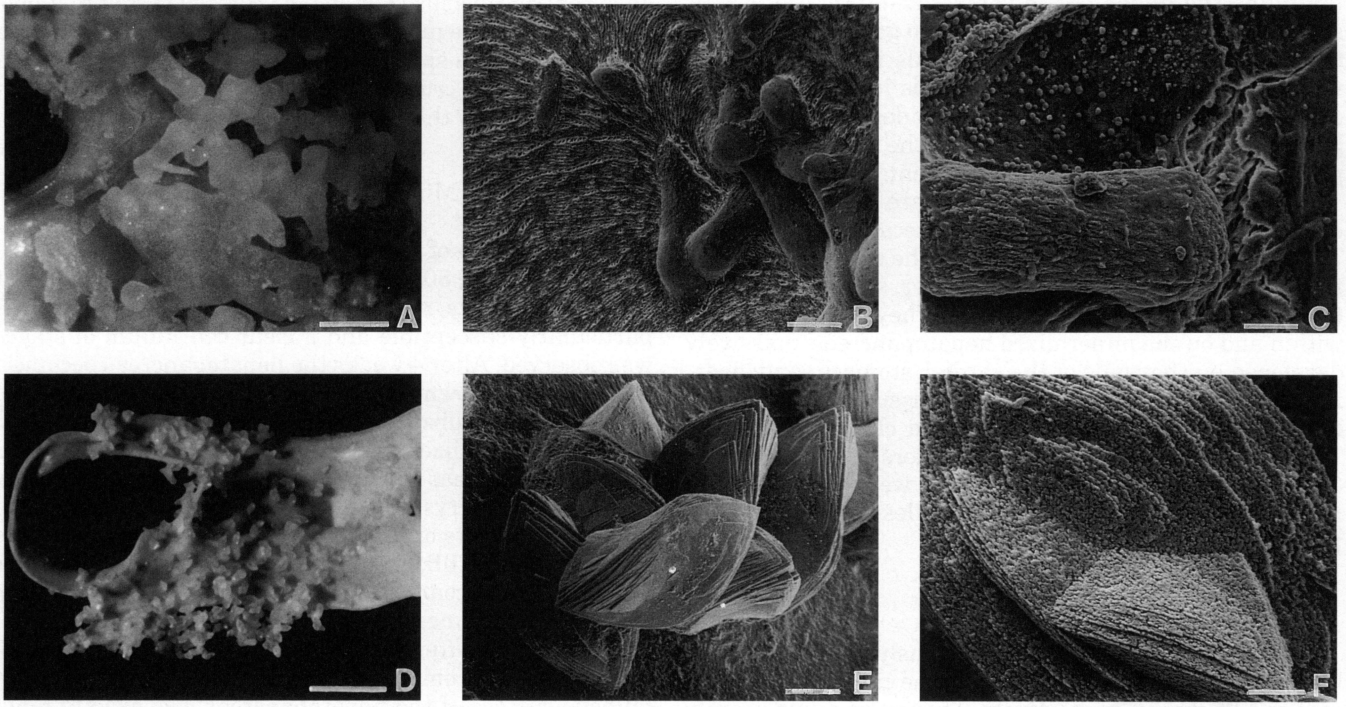

FIGURE 7—Styles of $CaCO_3$ mineralization. (A) Dumbbell-shaped crystal bundles on the inner surface of an abdominal sternite (8 weeks). Scale bar is 0.5 mm. (B,C) SEM illustrations. (B) Dumbbells on the inner surface of a sternite (8 weeks). Scale bar is 40 μm. (C) Detail of dumbbell on the inner surface of a sternite. Scale bar is 10 μm. (D) Almond-shaped crystal bundles on the inner surface of an abdominal sternite (25 weeks). Scale bar is 0.9 mm. (E,F) SEM illustrations. (E) Detail from (D). Scale bar is 40 μm. (F) Detail of almond-shaped crystal bundle. Scale bar is 10 μm.

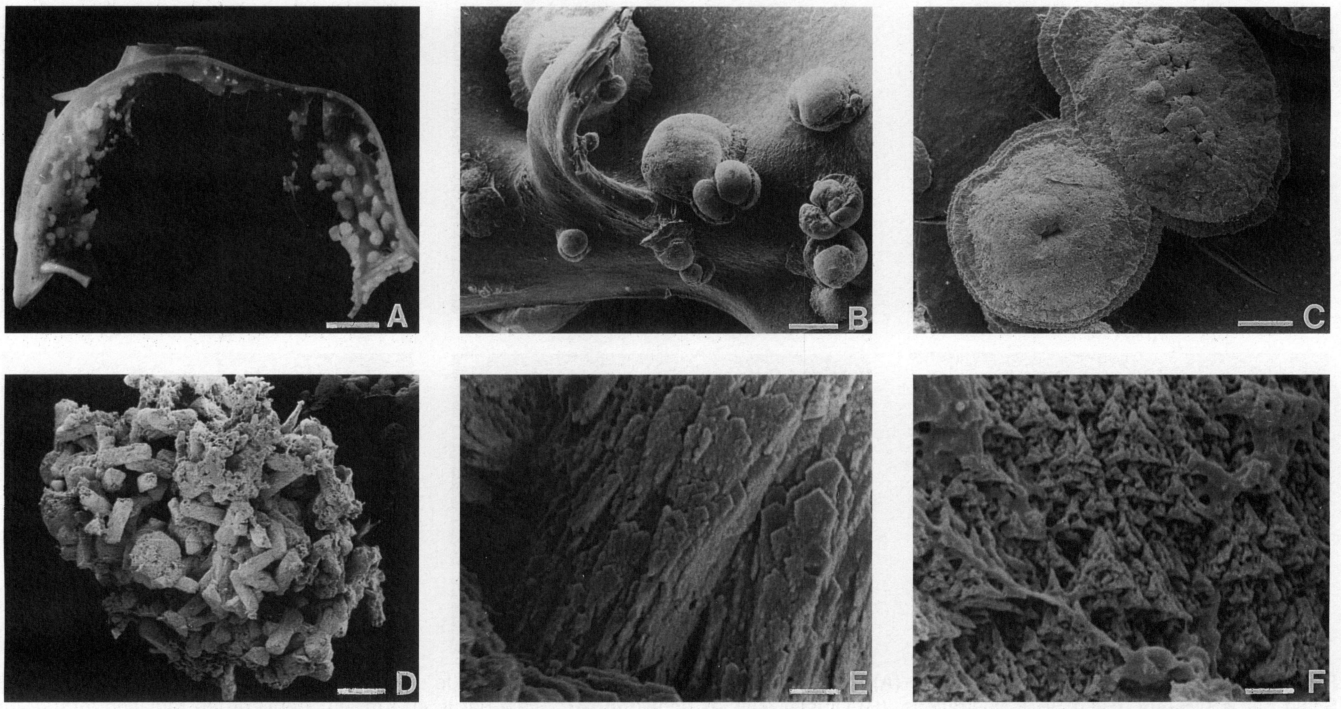

FIGURE 8—Styles of $CaCO_3$ mineralization. (A) Thoracic tergite showing hemispherical crystal bundles on the inner surface (8 weeks). The spheres precipitate mainly on the lateral parts of the tergite. Scale bar is 1 mm. (B-F) SEM illustrations (all 8 weeks). (B) Hemispherical crystal bundles on the inner surface of a thoracic sternite. Scale bar is 100 μm. (C) Crystal bundles on the inner surface of the mid-field of the carapace. Scale bar is 40 μm. (D) Cluster of crystal bundles from inside a telson. Scale bar is 100 μm. (E) Detail of the surface of a rod-shaped crystal bundle from (D). Scale bar is 4 μm. (F) Detail of the surface of a spherical crystal bundle from (D). Scale bar is 4 μm.

8E) and were whitish in color. Dumbbell-shaped crystal bundles were only observed in the abdominal sternites, often filling the lumen of the ventral keel (Fig. 7A, C). In some cases the dumbbells appeared to grow out of the cuticle (Fig. 7B). The individual crystals in the dumbbells were oriented parallel to the long axis in the neck of the dumbbell, and radiated out to varying degrees in the swollen extremities (Fig. 7C). Most of the dumbbells were pinkish in color and slightly translucent.

Almond-shaped crystal bundles were observed in only one experiment—a carcass that had decayed for 25 weeks. They formed on the inner surface of the cuticle, mostly on the trunk sternites (Fig. 7D). However, some grew on the tergites and median carapace field. They were also found within and on the mineralized hepatopancreas, massively developed on the walls of the cardiac stomach, and 'floating' between fragments of muscle tissue. These crystal bundles occurred solitary or in fused clusters (Fig. 7E). They were composed of leaf-like layers of microcrystals (Fig. 7F). These transparent crystals were light brown to reddish in color. Almond-shaped bundles have not been reported before.

Crystal Crusts

Crusts, which are composed of translucent $CaCO_3$ (Tables 2, 3) formed in 40% and 60% of the carcasses sampled at 8 and 25 weeks, respectively. They were found mainly on the outer surface of the trunk cuticle or the eye peduncles. Large flat rosette-shaped crusts (Fig. 6D) and irregular thin patches of crystals (Fig. 2C) were frequently observed on the median field of the abdominal tergites. Smaller, fragmented crusts formed on the margins of the tergites (Fig. 6D). Some of the rosettes radiated from a dark central nucleus (Fig. 6D, E) corresponding to a hole in the cuticle. The nucleus of some crystal crusts appeared to coincide with a spherical crystal on the inside of the cuticle. The crystal crust consisted of a thin basal layer, covered by a slightly thicker one (Fig. 6F).

Mineralized Soft-tissue

Mineralization of soft-tissue occurred in most of the experiments (in 20, 80, and 80% of the carcasses sampled at 4, 8, and 25 weeks, respectively). The hepatopancreas was particularly susceptible and a clear continuum of stages was observed. After 4 weeks the hepatopancreas became a hard, brittle, brown mass upon drying. This consisted of an amorphous substrate with clusters of small spheres, probably mineralized bacteria (Fig. 10A). After 8 weeks, the hepatopancreas survived in some specimens as a fragmented, brown, crystalline rod. This appeared to consist of amorphous sheets or plates, in which small spheres were embedded (Fig. 10B, C). Some pieces were whitish in color and made up of coarse granular crystalline material (Fig. 10D) that sometimes incorporated rod-shaped crystal bundles (Fig. 10E). After 25 weeks, large pieces of the hepatopancreas were completely mineralized. The irregularly bulbous surface of the hepatopancreas was exactly replicated (Fig. 10F). In some cases remains of the blood-veined epithelium that surrounds the hepatopancreas gave the mineralized remains a pinkish appearance. EM analyses of the hepatopancreas at different stages revealed a strik-

TABLE 2—Average composition of crystals and mineralized tissues in *Neogonodactylus oerstedii* (decay times in weeks). Oxide weights based on electron microprobe analyses (total given as weight percent of sample mineralized). Ratio of calcium phosphate to $CaCO_3$ based on the assumption that all P_2O_5 is incorporated into ideal OH-apatite [$Ca_5(PO_4)_3OH$]. The CaO : P_2O_5 ratio is 1:1.32 (based on molecular weights, ignoring H and excess O). The remaining CaO is assumed to form $CaCO_3$.

Material	Number of points analyzed	Weight percent of sample mineralized	Na_2O	MgO	SiO_2	P_2O_5	SO_3	CaO	CaO in amorphous phosphate	Ratio of phosphate to $CaCO_3$ (as percent)
Mineralized muscle (8w)	2	18.77	0.45	0.51	0.05	6.75	0.40	10.65	8.91	83.7 : 16.3
Crystal "dumbbells" (8w)	3	62.35	0.18	1.23	0	1.50	0.93	58.47	1.98	3.4 : 96.6
Crystal "white hemisphere" (8w)	2	62.66	0.15	1.50	0	1.45	0.80	58.70	1.91	3.2 : 96.8
Crystal "almond shaped" (25w)	6	54.32	0.18	0.18	0	2.07	0.17	51.80	2.73	5.3 : 94.7
Crystal "crust" (8w)	2	57.40	0.31	1.70	0	2.00	0.50	52.85	2.64	5.0 : 95.0
"Brown" hepatopancreas (8w)	4	13.89	0.72	0.32	0.16	2.05	1.05	9.55	2.71	28.4 : 71.6
"White coarse" hepatopancreas (8w)	4	17.91	1.20	0.83	0.09	5.83	0.73	8.95	7.70	86.0 : 14.0
"White fine" hepatopancreas (25w)	1	25.84	1.50	1.40	0.16	7.80	0.70	14.20	10.30	72.5 : 27.5

ing increase in the proportion of calcium phosphate as mineralization proceeded (Table 2).

Mineralized muscle fibers were common in the experiments sampled after 8 and 25 weeks. In undisturbed carcasses, white muscle layers were clearly visible through the transparent cuticle. These mineralized muscles were fragmented and scattered during filtering. Individual fibers were clearly recognizable (Fig. 11A). In some cases, both the fibers and the surrounding sarcolemma were mineralized (Fig. 11B). In some cases, tiny spheres were evident on the surface of the mineralized fibers, presumably representing mineralized bacteria (Fig. 11C). The outline of the sarcolemma was occasionally mineralized where the muscles attached to the cuticle (Fig. 13A,B). The mineralized muscles were composed of $CaPO_4$ (Table 2). In some cases, they contained $CaCO_3$ crystals or were overgrown by dumbbells (Fig. 11D), indicating a switch from $CaPO_4$ to $CaCO_3$ precipitation.

Even the nerve ganglion became mineralized, as revealed by one of the experiments sampled after 8 weeks (Fig. 11E). The composition of this delicate tissue was not analyzed. The surface of the nerve cell was covered with rhomb-shaped crystals (Fig. 11F), presumably of calcium carbonate.

Mineralization in the Cuticle

Currey et al. (1982) reported that the cuticle of the gonodactylid raptorial limb and telson seems to consist of two layers that differ in composition, structure and function. Calcium phosphate, as opposed to hydroxyapatite, is the major constituent of the surface layers. The balance of the

TABLE 3—Average composition of fresh, decayed, and mineralized cuticle in *Neogonodactylus oerstedii* (decay times in weeks) (see Fig. 12 and column 3 below for locations). Oxide weights based on electron microprobe analyses (total given as weight percent of sample mineralized). Ratio of calcium phosphate to $CaCO_3$ based on the assumption that all P_2O_5 is incorporated into ideal OH-apatite [$Ca_5(PO_4)_3OH$]. The CaO : P_2O_5 ratio is 1:1.32 (based on molecular weights, ignoring H and excess O). The remaining CaO is assumed to form $CaCO_3$.

Material	Number of points analyzed	Location in Fig. 12	Weight percent of sample mineralized	Na_2O	MgO	SiO_2	P_2O_5	SO_3	CaO	CaO in amorphous phosphate	Ratio of phosphate to $CaCO_3$ (as percent)
Endocuticle tergite (fresh)	1	A: EN	35.57	0.70	1.70	0.44	3.00	0.80	27.50	3.96	14.4 : 85.6
Exocuticle tergite (fresh)	1	A: EX	51.31	0.43	3.10	0	4.50	0.40	42.90	5.94	13.8 : 86.2
Endocuticle sternite (fresh)	2		26.55	0.43	1.22	0	5.30	0.70	18.70	6.99	37.4 : 62.6
Exocuticle sternite (fresh)	2		52.70	0.55	2.65	0	6.20	0.40	42.70	8.18	19.2 : 80.8
Endocuticle tergite (25w)	2	B: EN	28.52	0.73	1.85	0.13	9.70	1.80	13.80	12.80	92.7 : 7.3
Exocuticle tergite (25w)	2	B: EX	45.76	1.25	3.45	0.77	14.55	1.60	23.10	19.21	83.2 : 16.8
Crystal crust on tergite (8w)	1	C: arrow	55.48	0.29	1.10	0	1.80	0.80	51.50	2.38	4.6 : 95.4
Exocuticle tergite (8w)	2	C: EX	54.27	0.90	1.45	0	19.10	1.15	30.05	25.21	83.9 : 16.1
Endocuticle tergite (8w)	2	C: EN	52.26	0.95	1.40	0.02	18.45	0.90	29.30	24.35	83.1 : 16.9
Crystal inner side tergite (8w)	2	C: ci	59.01	0.28	1.30	0	1.90	0.70	54.85	2.51	4.6 : 95.4
Filled endocuticle (25 w)	3	D: EN	66.00	0.63	1.90	0	6.53	0.56	55.40	8.62	15.6 : 84.4
Exocuticle tergite (25w)	2	D: EX	42.99	1.55	1.90	0.05	13.45	0.55	24.00	17.75	74.0 : 26.0
Crystal crust on tergite (25w)	2	E: arrow	61.84	0.29	2.55	0	1.77	0.25	56.15	2.34	4.2 : 95.8
Completely mineralized sternite (25w)	4	F	65.95	0.33	1.65	0	3.93	0.83	58.55	5.19	8.9 : 91.1

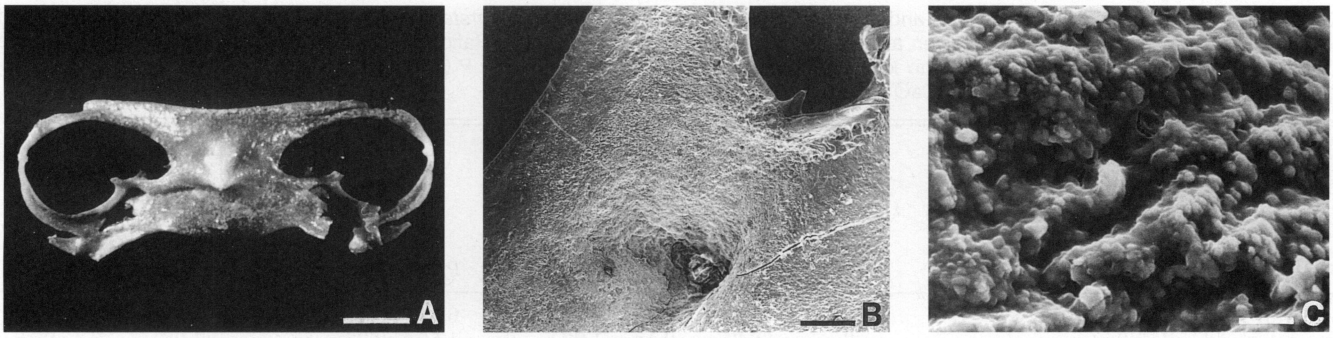

FIGURE 9—Completely mineralized sternite (25 weeks). (A) General view of outer surface. Scale bar is 1 mm. (B) SEM illustration of inner surface. Scale bar is 200 μm. (C) Detail from (B). Scale bar is 2 μm.

calcium is presumably calcium carbonate, with a small percentage of calcium sulphate (Currey et al., 1982). The high percentage of calcium phosphate in stomatopod cuticle is confirmed by comparison with other selected crustaceans (Richards, 1951; Plotnick, 1990).

The dried cuticle of freshly killed stomatopods is opaque, but throughout the decay experiments an irregular patchwork of opaque and transparent areas was apparent in dried cuticle, particularly in the tergites and sternites of the trunk. It is not clear whether these patterns were caused by mineralization of the cuticle, or by decay-induced structural changes in the cuticular layers.

Cross sections of the cuticle of trunk tergites and sternites of both fresh and decayed animals were photographed under back-scatter (Fig. 12) and analyzed (Table 3) in order to monitor changes with decay. The fresh cuticle clearly shows the endo- and exocuticular layers (Fig. 12A). Probe analyses (Table 3) reveal that the mineralized component of the exocuticle is higher than that of the endocuticle, in both tergite and sternites. In the tergites, however, there was no clear difference in the ratio of calcium phosphate to calcium carbonate in these two layers. In the sternites, the endocuticle contained relatively more phosphate than the exocuticle. This contrast to the result obtained by Currey et al. (1982) for the telson and raptorial limbs is presumably a reflection of different functions.

The back-scatter images revealed two distinct types of alteration of the cuticle during decay. First, degradation of the microfibrillar layers resulted in a loss of firmness (Fig. 12B) and separation of the cuticle layers (Fig. 12C). Second, calcium carbonate precipitated (visible in the back-scatter images as bright, white areas; Fig. 12C-F). Analysis of cuticle where no $CaCO_3$ precipitated showed an increase in the phosphate to carbonate ratio with decay in

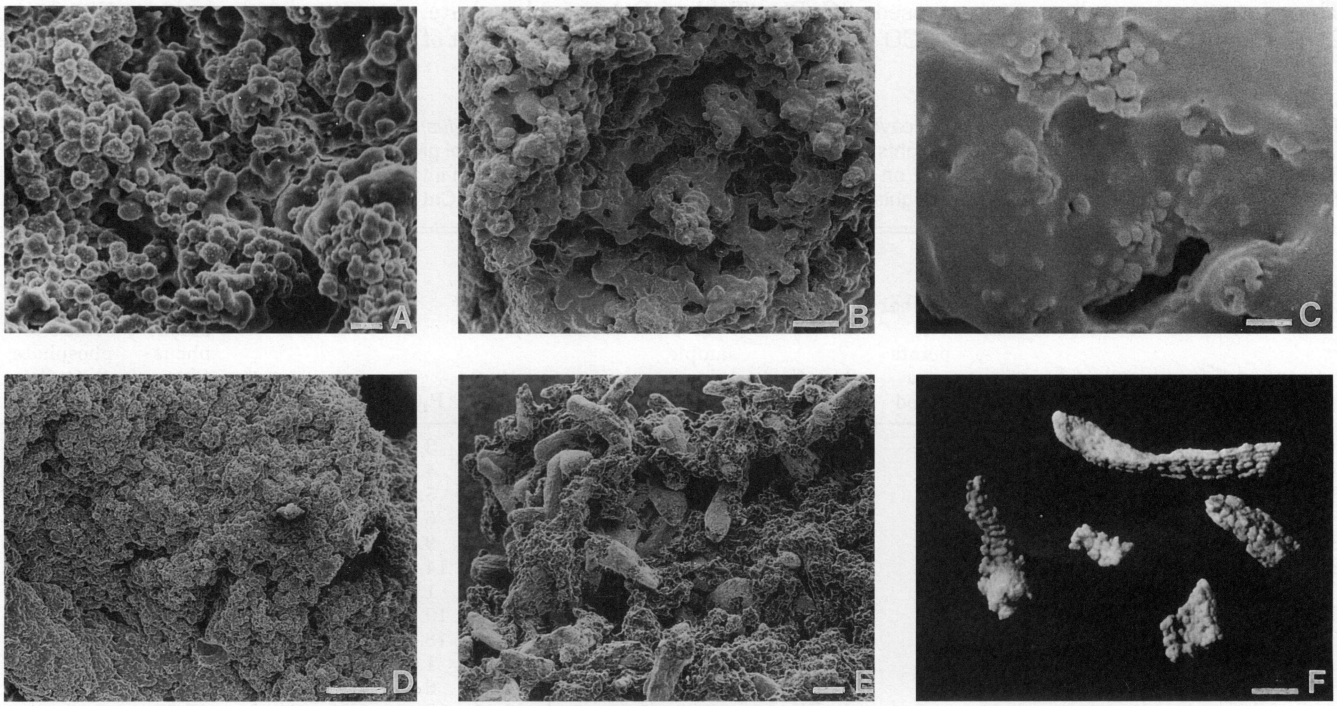

FIGURE 10—Hepatopancreas. (A-E) SEM illustrations. (A) Decaying surface (4 weeks). Scale bar is 4 μm. (B) Brown semi mineralized (8 weeks). Scale bar is 40 μm. (C) Detail from (B). Scale bar is 4 μm. (D) White coarse granular crystalline (8 weeks). Scale bar is 100 μm. (E) Crystalline with associated rod-shaped crystal bundles (8 weeks). Scale bar is 40 μm. (F) Completely mineralized, white, finely crystalline fragments showing the irregular bulbous surface (25 weeks). Scale bar is 1 mm.

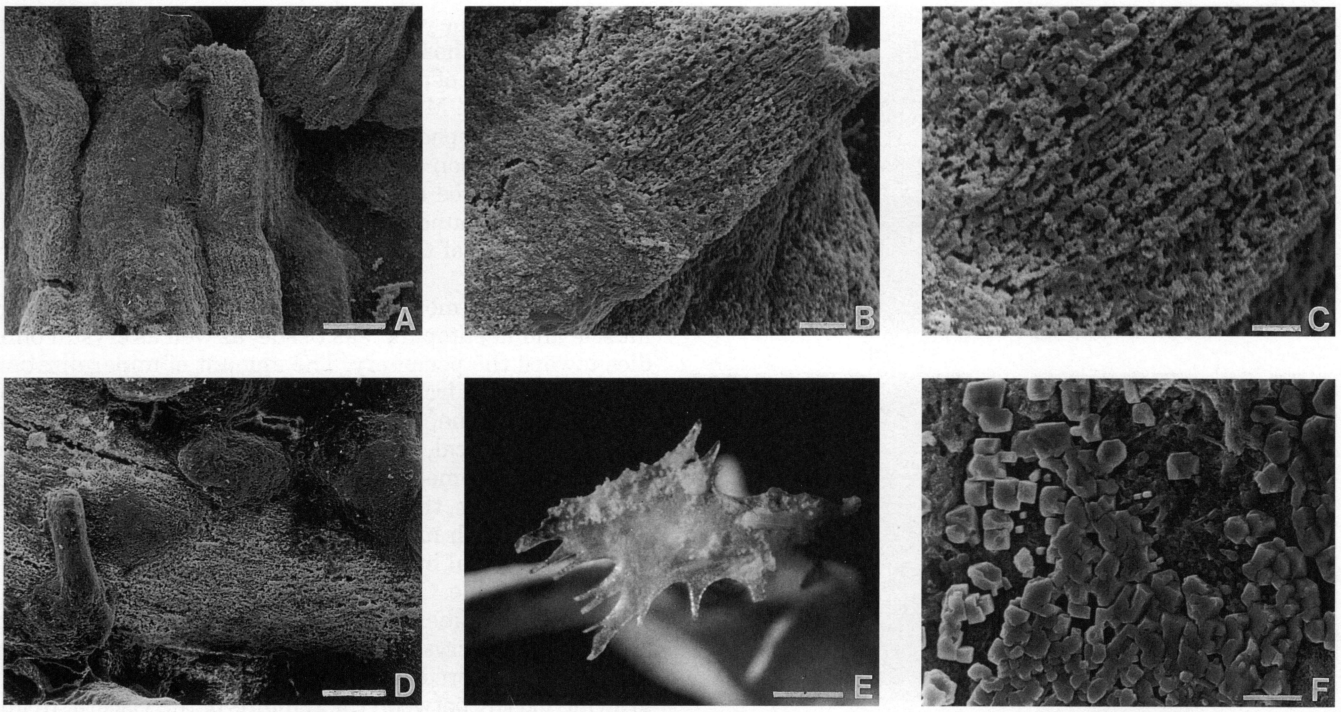

FIGURE 11—SEM illustrations (all 8 weeks). (A) Mineralized muscle fibers. Scale bar is 40 μm. (B) Detail of mineralized muscle fiber. Scale bar is 10 μm. (C) Detail of (B). Scale bar is 5 μm. (D) Mineralized muscle fiber overgrown by dumbbell-shaped crystal bundles. Scale bar is 40 μm. (E) Mineralized nerve ganglion. Scale bar is 0.15 mm. (F) Rhomb-shaped crystals on surface of mineralized ganglion. Scale bar is 4 μm.

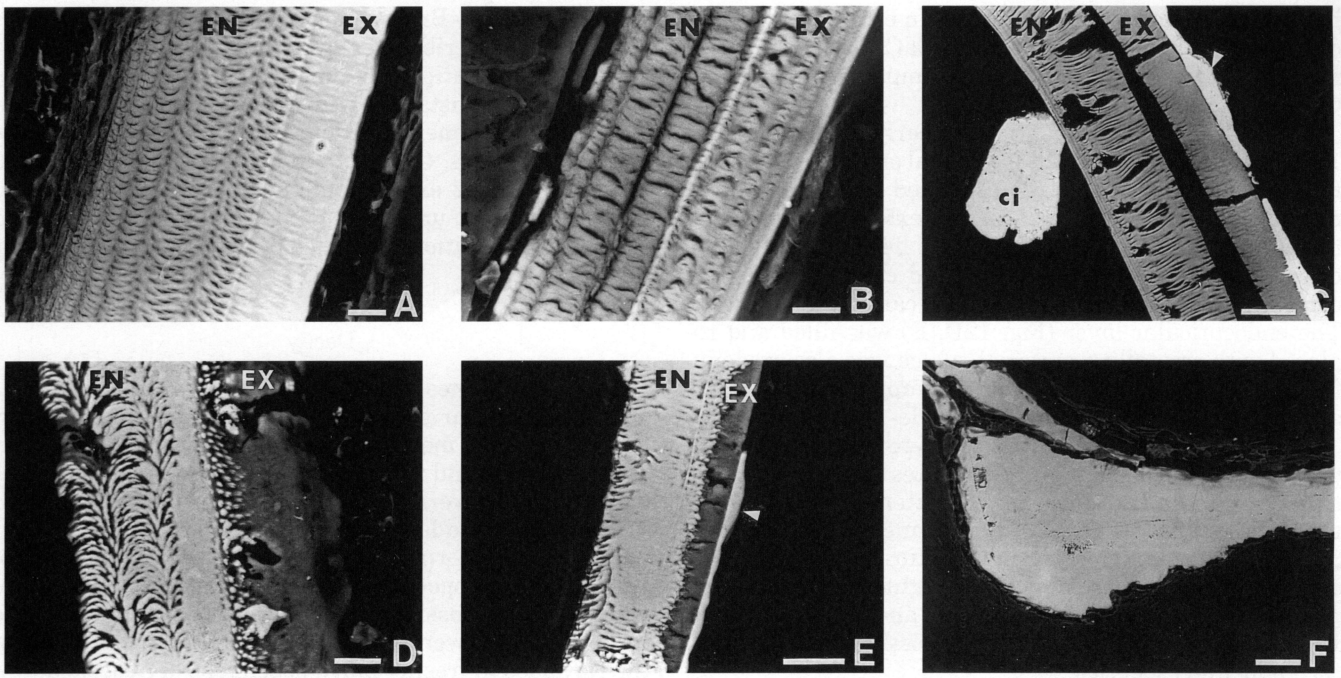

FIGURE 12—Back-scatter images of cross sections of cuticle (see Table 3 for analyses). (A) Fresh abdominal tergite showing the parabolic patterns evident in an oblique section of the helicoidal microfibrillar layers of the endocuticle (EN), and the more compact structure of the exocuticle (EX). Scale bar is 25 μm. (B) Abdominal tergite (25 weeks). Both endocuticle (EN) and exocuticle (EX) show a weakening of the structure. Scale bar is 20 μm. (C) Abdominal tergite (8 weeks), with a large solitary crystal bundle (ci) on the inner surface and a crystal crust (arrowed) on the outer surface. The effects of decay are evident in the exo- (EX), and endocuticle (EN). Scale bar is 50 μm. (D) Abdominal tergite (25 weeks), showing infilling of the endocuticular spaces with calcium carbonate (EN). Scale bar is 20 μm. (E) Abdominal tergite (25 weeks). Endocuticular spaces are infilled with calcium carbonate (EN) and a crystal crust (arrowed) is present on the outer surface. Scale bar is 40 μm. (F) Abdominal sternite (25 weeks). Cuticular layers are completely infilled and replaced with calcium carbonate. Scale bar is 50 μm.

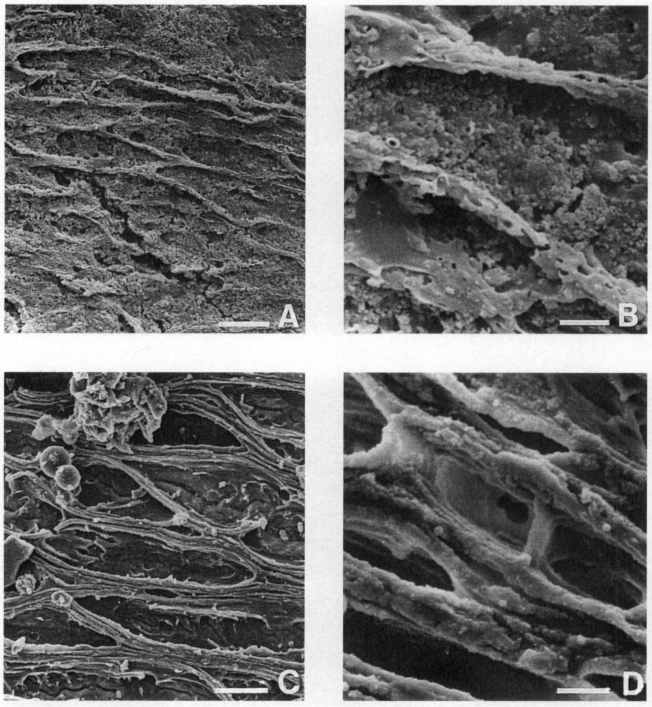

FIGURE 13—SEM illustrations of mineralized sarcolemma on the surface of the cuticle of decayed and fossil stomatopods. (A) Inner surface of the merus of a second thoracopod (8 weeks). Scale bar is 10 μm. (B) Detail of (A). Scale bar is 2 μm. (C) Inner surface of the dactylus of a fossil stomatopod (Miocene, California, USA). Scale bar is 10 μm. (D) Detail of (C). Scale bar is 2 μm.

both endo- and exocuticle (Table 3). In each case, the percentage of $CaPO_4$ exceeded that of $CaCO_3$ at least threefold, up to twelvefold. This was accompanied by a loss of Ca from the cuticle.

The pattern of mineralization is clearly shown in Figure 12. Figure 12C shows a solitary crystal on the internal surface of the cuticle, which corresponded in position to the nucleus of the crystal crust on the external surface (although the connection between them lies outside the line of section). Both solitary crystal and crystal crust were composed predominantly of calcium carbonate (Table 3). The endocuticular layer (Fig. 12D, E) was filled and replaced with crystalline material, which was also predominantly $CaCO_3$ (Table 3). This process appeared to be initiated at the boundary between the endo- and exocuticle.

One experiment resulted in complete mineralization of parts of the cuticle, mainly the sternites (Fig. 12F) and the trunk tergites, after 25 weeks. The outer surface of the cuticle became shiny (Fig. 9A), but the inner surface was dull and displayed a rough crystalline texture (Fig. 9B, C). This completely mineralized cuticle was light red in color, composed of calcium carbonate (Table 3), and was very brittle. In section (Fig. 12F), it is no longer possible to distinguish the endo- and exocuticle.

Patterns of Mineralization

Three aspects of the mineralization process were particularly striking: (1) the time that the minerals took to precipitate; (2) the frequent occurrence of $CaCO_3$ and $CaPO_4$ in the same carcass, usually in consistently different parts; and (3) the variability of mineralization between carcasses, even those sampled at the same time interval.

The first signs of mineralization were clearly evident after only 4 weeks. Muscle tissue inside the cuticular envelopes of the pleopods appeared to be mineralized in one carcass. The telson of the same individual was filled with spherical and rod-shaped crystal bundles (Fig. 8D-F). Hemispherical bundles were evident on the inner lateral surface of some of the abdominal tergites of another carcass.

After 8 weeks, most of the carcasses showed mineralized muscle and hepatopancreas tissue, as well as crystal bundles toward the periphery. The amount of mineralization varied, however, from extensive to just a few fragments of mineralized tissue, and from massively developed dumbbell, hemispherical, and rod-shaped crystal bundles (Figs. 7A, 8A) to just some very small crystal crusts and bundles.

After 25 weeks, the extent of mineralization was generally greater, with mineralized soft-tissues (Fig. 10F) and associated crystal bundles and crusts, although it continued to be variable. One carcass, which displayed well mineralized muscle fibers and hepatopancreas, also contained almond-shaped crystal bundles (Fig. 7D) emerging, either solitary or clustered, from the inner side of the cuticle, or growing loosely between the remains of the viscera. In another, no mineralized soft-tissue nor crystal bundles were observed but the cuticle (Figs. 9A, 12F) was shiny and brittle, and completely mineralized.

COMPARISON WITH EXPERIMENTS ON SHRIMPS

Previous experimental studies of crustacean taphonomy were reviewed by Briggs and Kear (1994, p. 449–451). The experiments described here were undertaken (1) as a basis for the interpretation of stomatopod fossils, and (2) to provide data on a crustacean with a more heavily mineralized cuticle to complement previous experimental work on the decapod shrimps *Crangon* and *Palaemon* (Briggs and Kear, 1994). The experiments on the decapods included some carried out under the same conditions (Briggs and Kear, 1994, condition 1c), which provide the main focus for comparison here.

Decay

The initial stages of morphological decay in the stomatopod were similar to those in shrimps. *Neogonodactylus,* however, proved more resistant to asphyxiation in anaerobic conditions and this may be reflected in a greater ability to survive adverse environments, including burial and suffocation by sudden influxes of sediment.

The unique morphology of the second pair of thoracopods in stomatopods provides a potential indicator of whether or not fossil specimens were buried alive. These raptorial claws were folded beneath the lateral fields of the carapace in freshly killed specimens of *Neogonodactylus*. Within 3 days, however, decay released the "click-joint" between the merus and carpus (Burrows, 1969; Burrows and Hoyle, 1972), resulting in unfolding. Osmotic uptake resulted in swelling of the stomatopod carcasses just as it did in shrimps. However, *Neogonodactylus* did not show the second phase of osmotic uptake at 2 weeks that was evident in *Crangon* (Briggs and Kear, 1994, fig. 6A).

The rise in wet weight evident after 8 weeks in *Neogonodactylus,* and to a lesser extent in *Crangon* (Briggs and Kear, 1994, fig. 6A), is not the result of osmosis. Given the variability of wet weights, it may be an experimental artifact.

The three stages of morphological decay—*Swollen, Ruptured,* and *Partially decomposed* (roughly equivalent to *Hollow* in shrimps)—observed in *Neogonodactylus* occurred in *Crangon* under equivalent conditions (Briggs and Kear, 1994, fig. 3, Condition 1c). The later stages of morphological decay (*Disarticulated, Fragmented*) recognized in shrimps were observed under different conditions to those in the decay experiments on *Neogonodactylus* (see Briggs and Kear, 1994, fig. 3). Nonetheless it is clear that the rate of decay of the stomatopod was slower. Statistical comparison of dry weights shows a significantly higher recovery in the stomatopod than in the shrimps. The rate of chemical degradation was also slower in the stomatopod ($P = 0.034$, two way ANOVA). TOC and H declined more gradually (Table 1), compared to the sudden decrease of these components in the shrimps (Briggs and Kear, 1994, table 4, figure 7). This difference in decay rate may reflect the larger proportion of decay-resistant chitin in the stomatopod. The sudden drop of N in both the stomatopod and shrimps is a consequence of the much more labile nature of proteins.

Crystal Bundles

A similar range of crystal bundle morphologies occurred in the stomatopod as in the shrimps (Briggs and Kear, 1994). The crystal crust that formed on the outside of the trunk tergites in several stomatopod carcasses, however, was not observed in the shrimps, and nor were the almond-shaped bundles that grew in just one individual. Crystal bundles and/or crystal crusts occurred in at least 80% of stomatopod carcasses sampled after 8 and 25 weeks. Although a precise comparison is not possible, it is clear that they formed more readily in the stomatopod than in the shrimps. However, they precipitated earlier in the latter under the same conditions (Briggs and Kear, 1994, fig. 12). Crystal bundles occurred routinely in the tergites and cephalothorax of the stomatopod, even though they were never recorded in this position in shrimps that decayed in the same closed conditions (1c of Briggs and Kear, 1994). In addition, crystal bundles normally formed in and on the cuticle of relatively large, central structures like the carapace, tergites, sternites and telson of the stomatopod in contrast to the peripheral positions such as in the scaphocerites, uropods, and chelae characteristic of their occurrence in the shrimps. Briggs and Kear (1994) regarded pH as the main control on whether $CaCO_3$ or $CaPO_4$ precipitated. The recovery of pH values to 7.5 following an initial drop (Fig. 4) might explain why crystal bundles only began to precipitate in the stomatopod after 4 weeks, but it does not account for their distribution within the carcasses. This may reflect pH values in particular parts of a decaying individual, which doubtless differed from the ambient pH in the experiment. The contrast in the abundance and distribution of crystal bundles in the stomatopod and shrimps may be a consequence of the higher content of $CaCO_3$ in the cuticle of the former.

Mineralized Soft-tissue

Various stomatopod soft-tissues became mineralized, but mainly the hepatopancreas and muscles. Just as in the similar experiments on shrimps, the soft-tissues were replicated by microspheres of $CaPO_4$. The replication of soft-tissue by calcium phosphate occurred more often in the stomatopod than in the shrimps. Whether or not this is significant is unclear due to discrepancies in both sample sizes and intervals. However, the occurrence of soft-tissue replication in 4 of the 5 stomatopods in the 8- and 25-week samples exceeds the 53% observed in the shrimps at 4, 6 and 8 weeks (Briggs and Kear, 1994).

The stages of soft-tissue replication were difficult to observe (Briggs and Kear, 1994). Muscle fibers were usually evident beneath the tergites, but they tended to disaggregate or float away when the carcass was disturbed during sampling, no matter how carefully the specimen was manipulated. This problem also arose with the hepatopancreas (Fig. 10A-F). Prior to mineralization, it appeared structureless simply because the partly decayed tissue lost coherence during sampling. The structure only survived where the carcass was left undisturbed long enough for mineralization to take place.

When muscle fibers were replicated, structural details were rarely preserved (Fig. 11A-C is the exception). Mineralized sarcolemma, such as that formed in the experiments on shrimps (Briggs and Kear, 1993b, 1994), was not common (Fig. 11B). The polygonal outlines of the sarcolemma where it inserts on the cuticle were preserved on the inner surface of the cuticle of the raptorial limb (Fig. 13A, B; compare Briggs and Kear, 1994, fig. 14I). The mineralization of a nerve ganglion (Fig. 11E), probably in $CaCO_3$, has only been observed in the stomatopod, not in shrimps. The rhomb-shaped crystals on the surface were similar to $CaCO_3$ rhombs found on decaying moults of shrimps (Briggs and Kear, 1994, fig. 13F).

Crystal bundles and mineralized soft-tissue occurred in the same carcass more frequently (60% in carcasses sampled at 8 and 25 weeks) than in the shrimps (15% in carcasses decayed in closed conditions sampled at 4 and 6 weeks). Occasionally dumbbells were observed overgrowing mineralized muscle fibers (Fig. 11D) as recorded in the shrimps (Briggs and Kear, 1994, fig. 19A), and rod- and almond-shaped crystal bundles were likewise observed on partly mineralized hepatopancreas (Fig. 10E).

Cuticle

The stomatopod cuticle, like that of the shrimps, became mineralized and it was also an important locus for the formation of crystal bundles. Thus the processes that affected it are critical to understanding the influence of the nature of the carcass on authigenic mineral formation. The few studies of stomatopod cuticle indicate that it differs in both structure and composition from that of other crustaceans. Krishnakumaran (1956) reported that the cuticle of *Squilla holoschista* (syn. *Oratosquilla holoschista*) differs from that of decapod crustaceans in possessing an outer endocuticle composed of fiber bundles or "Balken" lying between clearly defined lamellae. Dennell (1976), however, rejected this interpretation, finding the cuticle of *Squilla desmaresti* similar to general decapod cuticle. The en-

TABLE 4—State of preservation of all known Mesozoic and Tertiary stomatopod species

Taxon	Origin	Remarks
Complete (= swollen)		
Leesquilla bajee Yun, 1985	L.-M. Mio. Korea	2 specimens, dorso-ventral, 1 with raptorial claw unfolded
Shako tomidai Karasawa, 1996	L. Mio. Japan	2 specimens, 1 lateral, 1 dorso-ventral
Lysiosquilla antiqua (Münster, 1842)	L.-M. Eoc. Monte Bolca, Italy	numerous specimens, lateral and dorso-ventral
Sculda syriaca Dames, 1886	U. Cretaceous Hakel, Lebanon	few specimens, dorso-ventral
Pseudosculda laevis (Schlüter, 1874)	U. Cretaceous Hakel, Lebanon	numerous specimens, mainly lateral, raptorial claw unfolded
Squilla cretacea Schlüter, 1868	U. Cretaceous Sedenhorst Germany	1 specimen, raptorial claw unfolded (original lost?)
Paleosquilla brevicoxa Schram, 1968	M. Cretaceous Colombia	1 specimen, dorso-ventral
Sculda spinosa Kunth, 1870	U. Jurassic Solnhofen, Germany	3 specimens, all dorso-ventral
Sculda pusilla Kunth, 1870	U. Jurassic Solnhofen, Germany	1 specimen, dorso-ventral
Sculda pennata Münster, 1840	U. Jurassic Solnhofen, Germany	numerous specimens, all dorso-ventral
Partly complete (= ruptured)		
Chloridella sonomana Rathbun, 1926	Pli.? California, U.S.A.	posterior thorax and 6 abdominal somites
Pseudosquilla adelaidensis Rathbun, 1926	M. Mio. California, U.S.A.	abdomen with anterior part of telson
Phosquilla neonica Yun, 1985	L.-M. Mio. Korea	posterior abdomen with telson and part of uropods
Phosquilla scissodentica Yun, 1985	L.-M. Mio. Korea	posterior abdomen with telson and uropod
Leesquilla sunii Yun, 1985	L.-M. Mio. Korea	posterior thorax, abdomen, and telson
Squilla hollandi Förster, 1982	U. Eoc. Germany	carapace, flexed thorax and abdomen, + fragments
? *Pseudosquilla wulfi* Förster, 1982	U. Eoc. Germany	8 fragments of abdomen, 3 with carapace or telson
Bathysquilla wetherelli (Woodward, 1879)	Eoc. London Clay U.K.	5 specimens, mainly abdominal somites
Chloridella angolia Berry, 1939	Cretaceous Angola (Eoc.-Förster, 1982)	imprint of abdomen with uropods and telson
Lysiosquilla nkporoensis Förster, 1982	U. Cretaceous Nigeria	3 fragments of abdomen (1 + telson), and 1 carapace
Fragmentary (= partially decomposed)		
Chloridella empusa Rathbun, 1935	Pleist. Maryland, U.S.A.	1 telson and 1 dactyl of raptorial claw
Gonodactylus oerstedii Rathbun, 1935	M. Mio. North Carolina U.S.A.	basal prolongation of right uropod
Squilla miocenica Lovisato, 1894	M. Mio. Italy and Spain	6 specimens with only dactyls of the raptorial claw
Oratosquilla? sp. Karasawa and Nakagawa, 1992	M. Mio. Japan	dactyl of raptorial claw
Squilla sp. Yun, 1985	L.-M. Mio. Korea	fragment of telson

docuticle of *Neogonodactylus* (Fig. 12A) does not show a "Balken" structure as defined in Richards (1951, p. 192–194). Clearly visible are the parabolic patterns evident in an oblique section of helicoidal microfibrillar layers (Fig. 12A). A helicoidal architecture is universal in arthropod cuticle and has been reported, for example, in the decapods *Astacus* and *Homarus* and the fossil lobster *Eryma stricklandi* (Neville, 1975; Neville and Berg, 1971).

Comparison of the composition of fresh stomatopod cuticle (Table 3) with that of fresh shrimp cuticle (Table 5 of Briggs and Kear, 1994) confirmed the relatively high percentage of calcium phosphate in the former. Several lines of evidence showed that the cuticle is a site of diagenetic change: cloudy patterns developed within it; crystal bundles appeared to grow out of it; and changes occurred in its composition (Table 3) leading ultimately to mineralization of the cuticle itself. Briggs and Kear (1994) found a similar increase in the phosphate content of decayed shrimp cuticle. The 'calcification' of the stomatopod cuticle observed in these experiments appeared to be the result of a process independent of the observed phosphate increase, just as the formation of crystal bundles was independent of the mineralization of muscle tissues elsewhere in the carcass.

TAPHONOMY OF FOSSIL STOMATOPODS

About 400 extant species of stomatopod are known, and the taxonomy of the group, which has recently been the subject of major revision (Manning, 1995), is stable. Their fossil record, however, is poor and fragmentary. Schram (1986) recognized two suborders of stomatopod: the Unipeltata, which accommodates the living taxa and those of the Mesozoic and Tertiary, and the Archaeostomatopodea, which is Paleozoic. All the families within the Unipeltata, apart from the Sculdidae, have living representatives. Only one family of Archaestomatopodea, the Tyrannophontidae, is currently recognized (Schram, 1984). Many fossil stomatopods are based on imperfectly preserved material.

Berry (1939) comprehensively summarized the taxonomic history of the Sculdidae and other fossil stomatopods known at that time. Holthuis and Manning (1969) reviewed the fossil stomatopods, indicating the uncertain affinities of most of them. More recently, important fossil occurrences have been reported from the Tertiary of

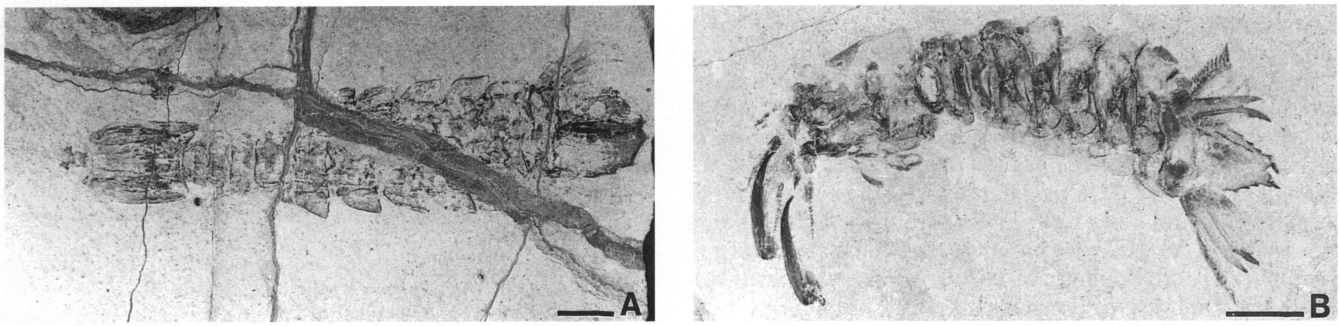

FIGURE 14—Fossil stomatopods, dorso-ventrally flattened. (A) Fossil stomatopod (Miocene, California, USA) with the raptorial claws folded underneath the carapace. Scale bar is 10 mm. (B) *Pseudosculda laevis* (Cenomanian, Hakel, Lebanon) showing unfolded raptorial claws (in a slightly oblique orientation). Scale bar is 5 mm.

Germany (Förster, 1982; Lienau, 1985), Korea (Yun, 1985), and Japan (Karasawa and Nakagawa, 1992; Karasawa, 1996), and the Early Maastrichtian of Nigeria (Förster, 1982).

The Mesozoic and Tertiary stomatopod fossils are the most useful for comparison with the results of the experiments (Table 4). Nonetheless, the descriptions of most taxa based on complete specimens date from the end of the last century and many are in need of revision. In addition, the taphonomic information that can be obtained from the literature and museum collections is inevitably biased by selective collecting. However, the stages of morphological decay discerned in the experiments can be recognized. Fossil specimens can be categorized as complete, partly complete or fragmentary, which correspond to the morphological decay stages *Swollen, Ruptured* and *Partially decomposed,* respectively (Table 4). A survey of Mesozoic and Tertiary fossil stomatopods revealed that the proportion of species based on material in these three categories is approximately 40% complete, 40% ruptured, and 20% fragments.

(1) *Complete (Swollen)*—In freshly killed animals, the raptorial thoracopods were folded underneath the carapace but they unfolded within 3 days as a result of decay. Thus, fossil specimens that show these appendages folded (Fig. 14A) were presumably buried alive or at least undisturbed (the limbs may be prevented from unfolding, however, where the specimen is oriented with the dorsal surface parallel to bedding). Unfolding clearly indicates that the muscles operating the "click-joint" between the merus and carpus had started to decay (Fig. 14B).

Lysiosquilla antiqua is one of the most completely known fossil stomatopods (Secretan, 1975). The collection of about 50 specimens in the Museo Civico di Storia Naturale di Verona (under study by C.H.J.H.) shows many of the features observed in the decay experiments: folded (Secretan, 1975, pl. 26, figs. 1,2) and unfolded (pl. 32, fig. 1; pl. 35, figs. 3,4) raptorial claws; swelling between the thoracic and abdominal somites due to osmotic uptake (pl. 31, figs. 1–3); and rupture of the trunk often between the fifth and sixth abdominal somite (pl. 30, fig. 2; pl. 32, figs. 1,4). Traces of mineralized soft-tissue are clearly evident in the abdomen, enclosed by the mineralized remains of the sternites and tergites. Remnants of muscle tissue (mainly sarcolemma) have also been observed on the innerside of the dactylus of the raptorial claw of a new stomatopod from the Miocene of California (Fig. 13C, D) (Hof and Schram, in press). These features are almost identical to sarcolemma mineralized in our experiment (Fig. 13A, B).

(2) *Partly complete (Ruptured)*—Many fossil stomatopods show the result of partial decomposition or fragmentation (Table 4). The arthrodial membranes almost always rupture within the posterior thorax, or between the thorax and abdomen, resulting in specimens comprised of the abdominal somites, sometimes with parts of the thoracic segments, carapace, or telson still attached. Rupture within the abdomen leaves the telson with only the sixth abdominal somite attached.

(3) *Fragmentary (Partially decomposed)*—Decay and fragmentation may destroy all but the more robust parts of stomatopods. Loose dactyli, for example, with or without the propodus, are heavily mineralized and are easily separated from the rest of the carcass during transport. They are the most common fragmentary remains of fossil stomatopods (Table 4).

Unequivocal crystal bundles have yet to be observed in fossil stomatopods, even though they occur in decapod shrimps from some of the same localities (e.g., Solnhofen: Briggs and Wilby, 1996). Their widespread formation in the experiments, however, even in closed conditions which inhibited their formation in shrimps (Briggs and Kear, 1994), indicates that they may be concealed by the more robust cuticle of fossil stomatopods.

CONCLUSIONS

The experiments show that under closed, anaerobic conditions, the formation of calcium carbonate crystal bundles, and the replication of soft-tissue by calcium phosphate, occur extensively in decaying carcasses of the stomatopod *Neogonodactylus oerstedii.* These remarkable results confirm those of previous experiments using the decapod shrimps *Crangon* and *Palaemon* (Briggs and Kear 1993, 1994a). Several lines of evidence show that the cuticle is an important site of diagenetic change leading ultimately to mineralization of the cuticle itself. The different mineralization patterns observed in decaying decapod shrimps under the same experimental conditions confirms that differences in structural and chemical composition of crustaceans is an important factor in the process of early diagenetic mineralization (Briggs and Wilby, 1996). Although mineralization was more widespread in stomatopods than in shrimps, the experimental results showed

considerable variation. More detailed experiments are essential to reveal the sources of such variability.

The stages of morphological decay observed in *Neogonodactylus* can be recognized in fossil stomatopods. The preserved state of the second thoracopods and the degree of fragmentation of the body are strongly time-related taphonomic features. Mineralized soft-tissue occurs in fossil stomatopods and more extensive examination of available material will certainly reveal important new information. Despite the relatively high mineralization potential of stomatopods, their fossil record is poor and fragmentary. 60% of Mesozoic and Tertiary species, for example, are based on ruptured or fragmentary specimens. This may reflect low taxonomic diversity in the past, or be a function of taphonomic and ecologic factors. Only further research can distinguish between these alternatives.

ACKNOWLEDGMENTS

We are grateful to A.J. Kear and P.R. Wilby for advice and discussion. We thank R.J. Parkes, B.A. Cragg and colleagues (microbiology), D.F.R. Cleary (statistics), T. Dekkers (C:H:N analysis), S. Lane (electron microprobe), S. Powell (SEM and photography) and D.M. Unwin (macrophotography with binocular microscope) for assistance. N.J. Marshall, the late Jeremy Jones, and J.M. Horwood from the Sussex Centre for Neuroscience kindly coordinated the supply of animals. M.F. Claridge, University of Wales, and F.R. Schram, University of Amsterdam, cooperated in setting up our study. R.E. Plotnick and an anonymous referee offered useful comments on an earlier version. The work was partly funded by The British Council, ref. NET/2281/99. It was completed during DEGB's tenure of a University of Bristol Staff Research Fellowship.

REFERENCES

ALLISON, P.A., 1986, Soft-bodied animals in the fossil record: The role of decay in fragmentation during transport: Geology, v. 14, p. 979–981.

ALLISON, P.A., 1988, The role of anoxia in the decay and mineralization of proteinaceous macro-fossils: Paleobiology, v. 14, p. 139–154.

BAAS, M., BRIGGS, D.E.G., VAN HEEMST, J.D.H., KEAR, A.J., and DE LEEUW, J.W., 1995, Selective preservation of chitin during the decay of shrimp: Geochimica et Cosmochimica Acta, v. 59, p. 945–951.

BEHRENSMEYER, A.K., and KIDWELL, S., 1985, Taphonomy's contributions to paleobiology: Paleobiology, v. 11, p. 105–119.

BERRY, C.T., 1939, A summary of the fossil Crustacea of the Order Stomatopoda, and a description of a new species from Angola: American Midland Naturalist, v. 21, p. 461–471.

BISHOP, G.A., 1981, Occurrence and fossilization of the *Dakoticancer* assemblage, Upper Cretaceous Pierre shale, South Dakota: *in* GRAY, J., BOUCOT, A.J. and BERRY, W.B.N., eds., Communities of the past: Hutchinson and Ross, Stroudsburg, Pa., p. 383–413.

BRETT, C., and BAIRD, G., 1986, Comparative taphonomy: A key to paleoenvironmental interpretation based on fossil preservation: PALAIOS, v. 1, p. 207–227.

BRIGGS, D.E.G., and KEAR, A.J., 1993a, Decay and preservation of polychaetes: Taphonomic thresholds in soft-bodied organisms: Paleobiology, v. 19, p. 107–135.

BRIGGS, D.E.G., and KEAR, A.J., 1993b, Fossilization of soft-tissue in the laboratory: Science, v. 259, p. 1439–1442.

BRIGGS, D.E.G., and KEAR, A.J., 1994, Decay and mineralization of shrimps: PALAIOS, v. 9, p. 431–456.

BRIGGS, D.E.G., and WILBY, P.R., 1996, Authigenic mineralization of soft-bodied fossils: the calcium carbonate/calcium phosphate switch: Journal of the Geological Society of London, v. 153, p. 665–668.

BRIGGS, D.E.G., KEAR, A.J., MARTILL, D.M., and WILBY, P.R., 1993, Phosphatization of soft-tissue in experiments and fossils: Journal of the Geological Society of London, v. 150, p. 1035–1038.

BUCZYNKSI, C., and CHAFETZ, H.S., 1991, Habit of bacterially induced precipitates of calcium carbonate and the influence of medium viscosity on mineralogy: Journal of Sedimentary Petrology, v. 61, p. 226–233.

BURROWS, M., 1969, The mechanics and neural control of the prey capture strike in the mantid shrimps *Squilla* and *Hemisquilla*: Zeitschrift für vergleichende Physiologie, v. 62, p. 361–381.

BURROWS, M., and HOYLE, G., 1972, Neuromuscular physiology of the strike mechanism of the mantis shrimp *Hemisquilla*: Journal of Experimental Zoology, v. 179, p. 379–394.

CALDWELL, R., and DINGLE, H., 1975, Ecology and evolution of agonistic behavior in stomatopods: Naturwissenschaften, v. 62, p. 214–222.

CALDWELL, R., and DINGLE, H., 1976, Stomatopods: Scientific American, v. 234 (1), p. 80–89.

CRAGG, B.A., BALE, S.J., and PARKES, R.J., 1992, A novel method for the transport and long term storage of cultures and samples in an anaerobic atmosphere: Letters in Applied Microbiology, v. 15, p. 125–128.

CURREY, J.D., NASH, A., and BONFIELD, W., 1982, Calcified cuticle in the stomatopod smashing limb: Journal of Materials Science, v. 17, p. 1939–1944.

DAMES, W., 1886, Über einige Crustaceen aus dem Kreideablagerungen des Libanon: Zeitschrift deutschen Geologischen Gesellschaft, v. 38, p. 551–575.

DENNELL, R., 1976, The cuticle of the hoplocarid crustacean *Squilla desmaresti* Risso: Zoological Journal of the Linnean Society, v. 62, p. 309–316.

FORSTER, R., 1982, Heuschreckenkrebse (Crustacea, Stomatopoda) aus dem Alttertiär von Helmstedt und Handorf (Niedersachsen) und der Oberkreide von Nigeria: Neues Jahrbuch für Geologie und Paläontologie, Monatshefte, 1982, p. 321–335.

GLAESSNER, M.F., 1929, Zur Kenntnis der Hautung bei fossilen Krebsen: Palaeobiologica, v. 2, p. 49–56.

HANSEN, H.J., 1895, Isopoden, Cumaceen und Stomatopoden der Planktonexpedition: Ergebnisse Planktonexpedition Humboldt-Stiftung, 2 (Gc), p. 1–105.

HOF, C.H.J., and SCHRAM, F.R., in press, Stomatopods (Crustacea: Malacostraca) from the Miocene of California: Journal of Paleontology.

HOLTHUIS, L.B., and MANNING, R.B., 1969, Stomatopoda: *in* MOORE, R.C., ed., Treatise on Invertebrate Paleontology, Part R, Arthropoda 4 (2): Geological Society of America and University of Kansas Press, New York and Lawrence, Kansas, p. R535-R552.

KARASAWA, H., 1996, *Shako*, a new Miocene stomatopod Crustacea from Japan: Transactions and Proceedings of the Palaeontological Society of Japan, v. 182, p. 413–418.

KARAWAWA, H., and NAKAGAWA, T., 1992, Miocene crustaceans from Fukui and Ishikawa Prefectures, central Japan: Bulletin of the Japan Sea Research Institute, v. 24, p. 1–18.

KRISHNAKUMARAN, A., 1956, On the structure and chemical nature of the cuticle in *Squilla holoschista* : Journal of the Zoological Society of India, v. 8, p. 171–178.

KUNTH, A., 1870, Über wenig bekannte Crustaceen von Solenhofen: Zeitschrift Deutsches Geologische Gesellschaft, v. 22, p. 771–790.

LIENAU, H.-W., 1985, Heuschreckenkrebse aus dem Geschiebe: Der Geschiebesammler, v. 19, p. 1–8.

LOVISATO, D., 1894, Avanzi di *Squilla* nel miocene medio di Sardegna: Rendiconti Accademia Lincei, Series 5, v. 3, p. 205–209.

LUCAS, J., and PRÉVÔT, L.E., 1991, Phosphates and fossil preservation: *in* ALLISON, P.A., and BRIGGS, D.E.G., eds., Taphonomy: Releasing the data locked in the fossil record: Plenum Press, New York, p. 389–409.

MANNING, R.B., 1969, Stomatopod Crustacea of the Western Atlantic: Studies in Tropical Oceanography no. 8, Institute of Marine Sciences, University of Miami, 380 p.

MANNING, R.B., 1995, Stomatopod Crustacea of Vietnam: The Legacy

of Raoul Serène: Crustacean Research, special number 4, The Carcinological Society of Japan, Tokyo, 339 p.

MERTIN, H., 1941, Decapode Krebse aus dem Subhercynen und Braunschweiger Emscher und Untersenon: Nova Acta Leopoldina, Neue Folge, v. 10, p. 149–263.

MÜLLER, A.H., 1979, Fossilization (Taphonomy): *in* ROBISON, R.A., and TEICHERT, C., eds., Treatise on Invertebrate Paleontology, Part A, Fossilization (Taphonomy) Biogeography and Biostratigraphy: Geological Society America and Kansas University Press, p. A2-A78.

MUNDLOS, R., 1975, Ökologie, Biostratinomie, und Diagenese brachyurer Krebse aus dem Alt-Tertiär von Helmstedt (Niedersachsen, BRD): Neues Jahrbuch für Geologie und Paläontologie, Abhandlungen, v. 148, p. 252–271.

MÜNSTER, G. GRAF ZU, 1840, über einige Isopoden in den Kalkschiefern von Bayern: Beitrage zur Petrefactenkunde, v. 3, p. 19–23.

MÜNSTER, G. GRAF ZU, 1842, Beschreibung drei neuer Arten Crustaciten: Beitrage zur Petrefactenkunde, v. 5, p. 76–77.

NEVILLE, A.C., 1975, Biology of the Arthropod Cuticle: Springer-Verlag, Berlin, Heidelberg, New York, 448 p.

NELVILLE, A.C., and BERG, C.W., 1971, Cuticle ultrastructure of a Jurassic crustacean *(Eryma stricklandi)*: Palaeontology, v. 14, p. 201–205.

PLOTNICK., R.E., 1986, Taphonomy of a modern shrimp: Implications for the arthropod fossil record: PALAIOS, v. 1, p. 286–293.

PLOTNICK., R.E., 1990, Paleobiology of the arthropod cuticle: Short courses in Paleontology, no. 3, Paleontological Society, Knoxville, Tennessee, p. 177–196.

PLOTNICK, R.E., BAUMILLER, T., and WETMORE, K.E., 1988, Fossilization potential of the mud crab *Panopeus* (Brachyura: Xanthidae) and temporal variability in crustacean taphonomy: Palaeogeography, Palaeoclimatology, Palaeoecology, v. 63, p. 27–43.

RATHBUN, M.J., 1926, The fossil stalked-eyed Crustacea of the Pacific slope of North America: U.S. National Museum Bulletin 138, p. 136–138.

RATHBUN, M.J., 1935, Fossil Crustacea of the Atlantic and Gulf coastal plain: Geological Society of America, Special Paper 2, 160 p.

RICHARDS, A.G., 1951, The integument of Arthropods: University Press: Minnesota, 411 p.

RUTTENBERG, K.C., and BERNER, R.A., 1993, Authigenic apatite formation and burial in sediments from non-upwelling continental margin environments: Geochimica et Cosmochimica Acta, v. 57, p. 991–1007.

SCHÄFER, W., 1951, Fossilizations-Bedingungen brachyurer Krebse: Abhandlungen der Senckenbergischen Naturforschenden Gesellschaft, v. 485, p. 221–238.

SCHÄFER, W., 1972, Ecology and Paleoecology of Marine Environments: University of Chicago Press, Chicago, 568 p.

SCHLÜTER, CL., 1868, Stomatopoda: *in* VON DER MARCK, W., and SCHLÜTER, CL., Neue Fische und Krebse aus der Kreide von Westphalen: Palaeontographica, v. 15, p. 303–304.

SCHLÜTER, CL., 1874, Über einige jurassische Crustaceen-Typen in der oberen Kreide. l. Fossile Krebse des Libanon: Sitzungsberichte herausgegeben vom naturhistorischen Verein der Preussischen Rheinlande und Westfalens, v. 31, p. 41–45.

SCHRAM, F. R., 1968, *Paleosquilla* gen. nov.—a stomatopod (Crustacea) from the Cretaceous of Colombia: Journal of Paleontology, v. 42, p. 1297–1301.

SCHRAM, F. R., 1984, Upper Pennsylvanian arthropods from black shales of Iowa and Nebraska: Journal of Paleontology, v. 58, p. 197–209.

SCHRAM, F. R., 1986, Crustacea: Oxford University Press, Oxford and New York, 606 p.

SECRETAN, S., 1975, Les crustacés du Monte Bolca: Studi e ricerche sui giacimenti terziari di Bolca, v. 2, p. 315–388.

WOODWARD, H., 1879, Contributions to the knowledge of fossil crustacea: Quarterly Journal of the Geological Society, v. 35, p. 549–551.

YUN, H., 1985, Some fossil Squillidae (Stomatopoda) from the Pohang Tertiary Basin, Korea: Journal of the Paleontological Society of Korea, v. 1, p. 19–31.

ACCEPTED NOVEMBER 18, 1996

APPENDIX

Raw data, means and standard deviations for decaying *Neogonodactylus oerstedii*: wet weights (WW), dry weights (DW) and pH. The last column identifies the animals that were used for specific analyses.

Time	Animal code	WW T = 0 (gr)	DW T = 0 (gr)	Final WW (gr)	Final DW (gr)	% WW left	% DW left	pH	Analyses
3 days	Mantis 21	0.932	0.348	0.877	0.200	94.12	57.65	6.63	N:C:H
	Mantis 22	0.997	0.372	1.288	0.232	129.27	62.37	6.58	SEM/EM
	Mantis 23	0.505	0.185	0.588	0.118	116.32	63.72	6.55	SEM/EM
	Mantis 24	0.857	0.319	–	–	–	–	6.72	future
	Mantis 25	1.722	0.648	2.079	0.456	120.73	70.28	6.34	Ca/PO_4
	average	1.003	0.375	1.208	0.252	115.10	63.51	6.56	
	stdv.	0.445	0.169	0.648	0.144	14.99	5.21	0.14	
1 week	Mantis 16	0.772	0.287	0.404	0.109	52.30	37.96	7.03	N:C:H
	Mantis 17	1.004	0.375	0.737	0.176	73.43	46.95	7.02	Ca/PO_4
	Mantis 18	0.973	0.363	0.586	0.152	60.21	41.92	7.11	SEM/EM
	Mantis 19	1.136	0.425	0.646	0.172	56.87	40.45	6.97	SEM/EM
	Mantis 20	1.154	0.432	–	–	–	–	7.04	future
	average	1.008	0.377	0.593	0.152	60.70	41.82	7.03	
	stdv.	0.154	0.059	0.141	0.031	9.08	3.79	0.05	
2 weeks	Mantis 11	1.115	0.417	0.280	0.108	25.12	25.95	7.07	SEM/EM
	Mantis 12	1.262	0.473	0.512	0.153	40.56	32.26	6.85	Ca/PO_4
	Mantis 13	0.881	0.328	–	–	–	–	6.72	future
	Mantis 14	1.117	0.418	0.568	0.142	50.87	33.88	6.90	N:C:H
	Mantis 15	0.491	0.180	0.107	0.046	21.69	25.52	6.58	SEM/EM
	average	0.973	0.364	0.367	0.112	34.56	29.40	6.82	
	stdv.	0.302	0.115	0.214	0.048	13.62	4.29	0.19	
4 weeks	Mantis 6	0.806	0.300	0.169	0.074	20.95	24.76	7.55	N:C:H
	Mantis 7	0.388	0.141	0.021	0.036	5.46	25.41	7.38	SEM/EM
	Mantis 8	1.408	0.529	0.690	0.157	49.01	29.63	7.50	SEM/EM
	Mantis 9	0.844	0.314	–	–	–	–	7.41	future
	Mantis 10	1.340	0.503	0.737	0.176	55.01	35.03	7.69	Ca/PO_4
	average	0.957	0.357	0.404	0.111	32.61	28.71	7.51	
	stdv.	0.421	0.160	0.363	0.067	23.41	4.73	0.12	
8 weeks	Mantis 26	1.430	0.537	0.544	0.201	38.02	37.34	7.98	SEM/EM
	Mantis 27	1.437	0.540	0.755	0.197	52.55	36.41	8.00	SEM/EM
	Mantis 28	1.421	0.534	–	–	–	–	8.01	future
	Mantis 29	1.276	0.479	0.732	0.192	57.37	40.00	8.07	Ca/PO_4
	Mantis 30	1.027	0.384	0.406	0.055	39.54	14.44	7.41	N:C:H
	average	1.318	0.495	0.609	0.161	46.87	32.05	7.89	
	stdv.	0.176	0.067	0.165	0.071	9.56	11.84	0.27	
25 weeks	Mantis 1	0.578	0.213	0.163	0.066	28.20	30.76	7.54	Ca/PO_4
	Mantis 2	0.793	0.295	–	–	–	–	7.52	future
	Mantis 3	0.773	0.287	0.224	0.112	29.02	39.14	7.67	N:C:H
	Mantis 4	1.908	0.719	0.876	0.345	45.93	48.01	7.74	SEM/EM
	Mantis 5	0.850	0.317	0.224	0.119	26.32	37.72	7.58	SEM/EM
	average	0.980	0.366	0.372	0.161	32.37	38.91	7.61	
	stdv.	0.529	0.201	0.338	0.125	9.11	7.08	0.09	